Geomorphology 103 (2009) 227–250

Contents lists available at ScienceDirect

Geomorphology

journal homepage: www.elsevier.com/locate/geomorph

Geomorphology of anomalously high glaciated mountains at the northwestern end of Tibet: Muztag Ata and Kongur Shan

Yeong Bae Seong [a,*], Lewis A. Owen [a], Chaolu Yi [b], Robert C. Finkel [c], Lindsay Schoenbohm [d]

[a] Department of Geology, University of Cincinnati, Cincinnati, OH 45221, USA
[b] Institute of Tibetan Plateau Research, Chinese Academy of Sciences, Beijing, 100085, China
[c] Center for Accelerator Mass Spectrometry, Lawrence Livermore National Laboratory, Livermore, CA 94550, USA
[d] Department of Geology, Ohio State University, Columbus, OH 43210, USA

ARTICLE INFO

Article history:
Accepted 15 November 2007
Available online 10 May 2008

Keywords:
Geomorphology
Northwestern Tibet
Quaternary
Terrestrial cosmogenic nuclides
Erosion rate
Topography

ABSTRACT

Muztag Ata and Kongur Shan massifs represent a significant area of anomalously high topography at the northwestern end of the Tibetan Plateau, rising to >7500 m above sea-level (asl) from the plateau that has an average elevation of ~3500 m asl. These massifs provide an excellent opportunity to test geomorphic concepts, such as the glacial buzz-saw model. Using remote sensing, digital elevation modeling, field mapping and terrestrial cosmogenic nuclide (TCN) methods, the massifs were examined to determine the relative importance of tectonics and geomorphic processes in shaping the regional landscape and to provide a framework for testing geomorphic models. The gneiss domes that underlie the peaks are the result of exhumation along the Kongur detachment fault that has unroofed the massifs at a rate of between 4–6 km/Ma over the last few million years. This has resulted in rapid uplift and active seismicity, which is exemplified by the numerous fresh fault scarps throughout the region and large historic earthquakes. The geomorphic system is dominated by glaciation and the region contains extensive successions of moraines and paraglacial landforms, including fans, terraces and landslides. Glaciers have oscillated considerably throughout the latter part of the Quaternary, and three major glacier stages are recognized (Karasu [oldest], Olimde and Subaxh [youngest] glacial stage) that include at least 10 smaller glacial advance. The style of glaciation has changed over time from expanded ice caps to piedmont glaciers to valley and cirque glaciers. This possibly reflects a change in climate and/or topographic constraints as the massifs grew and became incised. The topography and glaciers in the region vary across the massifs divided by a broadly N–S trending high ridge and watershed. The western portion, situated upwind (the stoss slopes) of the mid-latitude westerlies, that bring moisture to the region, has gentle high topography and small valley glaciers. In contrast, on the eastern leeward slopes, gradients are higher and long debris-covered valley glaciers are present. The hypsometry of the region indicate two peaks in the distribution frequency of elevation (3600–4100 m and 4400–4800 m asl). These two elevation zones are consistent in space with the former equilibrium-line altitudes during the Olimde and Subaxh glacial stages and suggest that glacial erosion (most effective at the ELA) has helped control topography. This observation supports the glacial buzz-saw hypothesis, which argues that glaciers determine hypsometry by means of rapid surface erosion. Based on TCN methods, basin-wide rates of erosion range from ~0.1 to 1.4 km/Ma and are five to ten times lower than the unroofing rate of both massifs. The discrepancy over different time scales suggests that initial unroofing was produced by abrupt tectonic uplift and that the unroofing of the massifs has continued at a slower pace during the Late Quaternary.

1. Introduction

Over the past decades, areas of significant anomalous topography, such as regions of the Himalaya (Molnar and England, 1990; Brozovich et al., 1997), Alaska (Meigs and Sauber, 2000; Spotila et al., 2004), the Andes (Montgomery et al., 2001), New Zealand (Koons, 1994), Cascade Range (Porter, 1989; Mitchell and Montgomery, 2006) and Sierra Nevada (Brocklehurst and Whipple, 2002, 2004) have attracted much attention to the role of glaciers in shaping the topography. Porter (1989) hypothesized that the erosional patterns of the landscape across the Cascade Range are linked to the distribution of the equilibrium-line altitudes (ELAs) and, thus, the efficacy of erosional processes must vary as a function of variations in glacier activity as forced by climate oscillation. Brozovich et al. (1997) suggested that the development of topography around Nanga Parbat is independent of the rate of tectonic uplift and is correlated with the focus of glacial and periglacial processes. This implies that glaciers exert a threshold on tectonic uplift and ultimately climate dominates

* Corresponding author. Present address: Department of Earth and Environmental Sciences, Korea University, Anam-Dong, Seongbuk-Gu, Seoul, 136-704, South Korea.
E-mail address: ybseong@hotmail.com (Y.B. Seong).

0169-555X/$ – see front matter © 2008 Elsevier B.V. All rights reserved.
doi:10.1016/j.geomorph.2008.04.025

landscape evolution. Montgomery et al. (2001) found that the topography of the southern Andes was primarily controlled by variations in precipitation and the degree of glaciation. Spotila et al. (2004) concentrated on the role of glacier as buzz-saw on the mountain building processes. They tested the hypothesis that glaciers rapidly erode topography that is above the equilibrium line altitude (ELA) and they place an upper altitudinal limit on how high mountains may be uplifted. This glacial buzz-saw model, as it has become known, has major implications for understanding the coupling between climate and topography in orogens. This hypothesis, however, has yet to be adequately tested because it is particularly challenging to distinguish, spatially and temporally, the closely interwoven effects of tectonics and glacial erosion.

At the northwestern end of the Tibetan Plateau, two high massifs, Muztag Ata and Kongur Shan, rise from the plateau that has an average elevation of ~3500 m asl to 7546 and 7719 m asl, respectively. Both massifs are ~1500 m higher than any of the neighboring peaks, and they represent an area of significant anomalously high topography (Figs. 1, 2, and 3; Schoenbohm et al., 2005). These massifs provide an opportunity to more readily isolate endogenetic and exogenetic processes, spatially and temporally, to help compare the impact of glaciers on landscape evolution. To begin to resolve the relative importance of endogenetic and exogenic processes in the Muztag Ata and Kongur Shan massifs and to provide a framework for future testing of the glacial buzz-saw model in the region, we describe the geomorphology of the massifs. We identify the dominant landforms and Earth surface processes that operate in the region. The relatively recent development of terrestrial cosmogenic nuclides (TCNs) methods to date landforms and to estimate rates of erosion allows quantification of landscape evolution (Brown et al., 1995; Granger et al., 1996; Clapp et al., 2000, 2001; Bierman and Caffee, 2001; Schaller et al., 2001; Matmon et al., 2003). Using these methods, we determine TCN concentrations in fluvial sediments and bedrock samples to help provide an outline of the recent geologic history of the massifs and to present the first estimates of the rates of Quaternary erosion. These are used to help construct a framework to determine the nature and dynamics of Quaternary landscape evolution in this region of anomalous topography.

2. Study area

Muztag Ata and Kongur Shan are situated in the Pamir–western Himalaya syntax that lies at the western end of the Indo-Asian collision zone, at the northwestern end of the Tibetan Plateau (Robinsion et al., 2004; Figs. 1 and 2). These are bounded to the north by the Main Pamir Thrust and to the south by Karakoram Fault. The Kongur detachment traverses the region and is a major extensional fault related to the exhumation of the Muztag Ata and Kongur Shan gneiss domes (Fig. 1B; Arnaud et al., 1993; Brunel et al., 1994; Robinsion et al., 2004; Robinson, 2005). Both domes are in the footwall of Kongur detachment, which has experienced rapid exhumation since 2 Ma (Arnaud et al., 1993). The region is seismically active and extensive surface ruptures and fault scarps provide visible evidence testifying to recent large earthquakes. The best examples of fault scarps are north of Muztag Ata where fresh surface ruptures trend westward through the Koqukalaq glacier. Other examples of fault scarps are present on the south-west side of Muztag Ata, where multiple strike–slip fault scarps trend southeast and cut across alluvial fans. These were probably the result of the 1885 Taghman earthquake (Magnitude is 7.5; Liu, 1993; Fort and Peulvast, 1995).

Climatologically, the Muztag Ata–Kongur Shan region is situated at the intersection of Indian summer monsoon and mid-latitude westerlies. At Bulun Kol (Fig. 2D; 38 44′ N, 75 02′E, 3310 m asl), the average annual temperature is 0.7 °C and the mean annual precipitation is 127 mm (during 1956 to 1968). The highest precipitation occurs between April and May as a result of the penetration of the mid-latitude westerlies into the region (Miehe et al., 2001). At Muztag Ata (Fig. 1; 38 42′ N, 75°01′ E, 5910 m asl), the precipitation supplied to the glacier accumulation zone during the summer is <30% of total annual amount (300 mm/yr at 5910 m asl). Most of precipitation is supplied by mid-latitude westerlies that bring moisture from the Mediterranean, Black Sea, and Caspian Sea (Aizen and Aizen, 1997; Barry and Chorley, 2003), and reach a maximum in spring (March to May; Fig. 2F). Wake et al. (1994) found that the annual maximum concentrations of particles in snow occurs once per year and represent the influx of dust during spring dust storms at the time of the peak precipitation

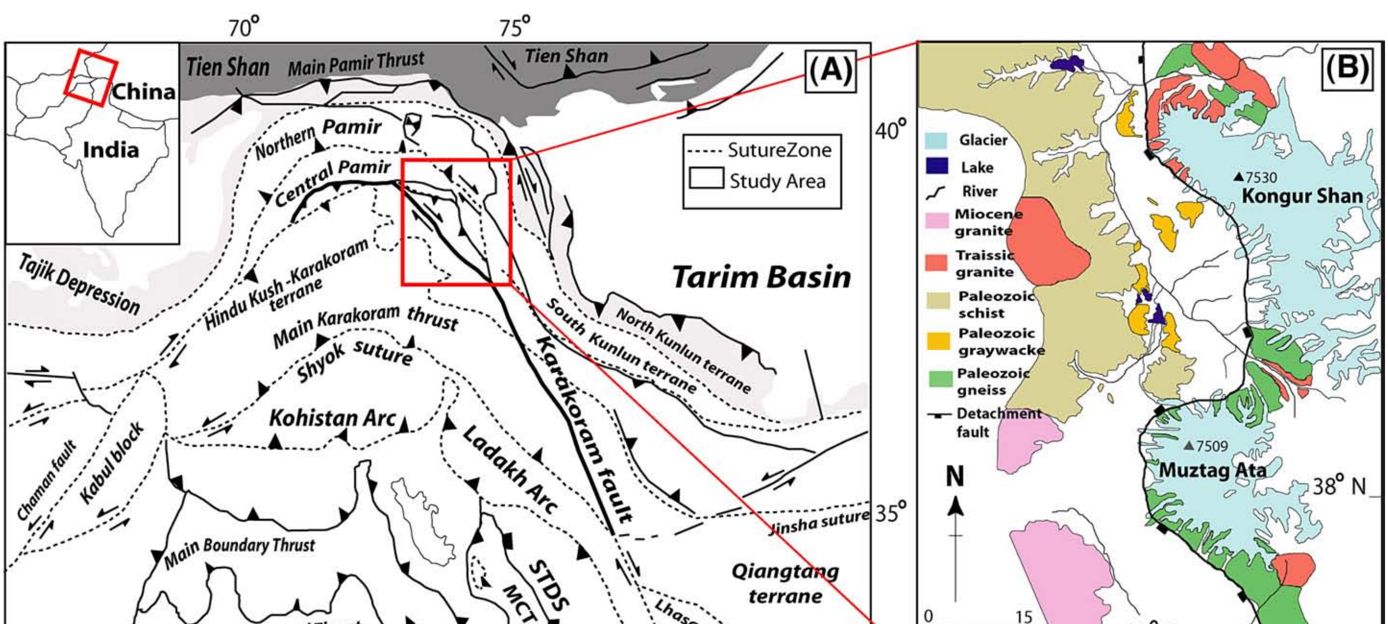

Fig. 1. Tectonic map of the western Tibet (A; modified from Robinsion et al., 2004; STDS — South Tibetan Detachment, MCT — Main Central Thrust) and geologic map of Muztag Ata and Kongur Shan. (B; modified from Robinson, 2005).

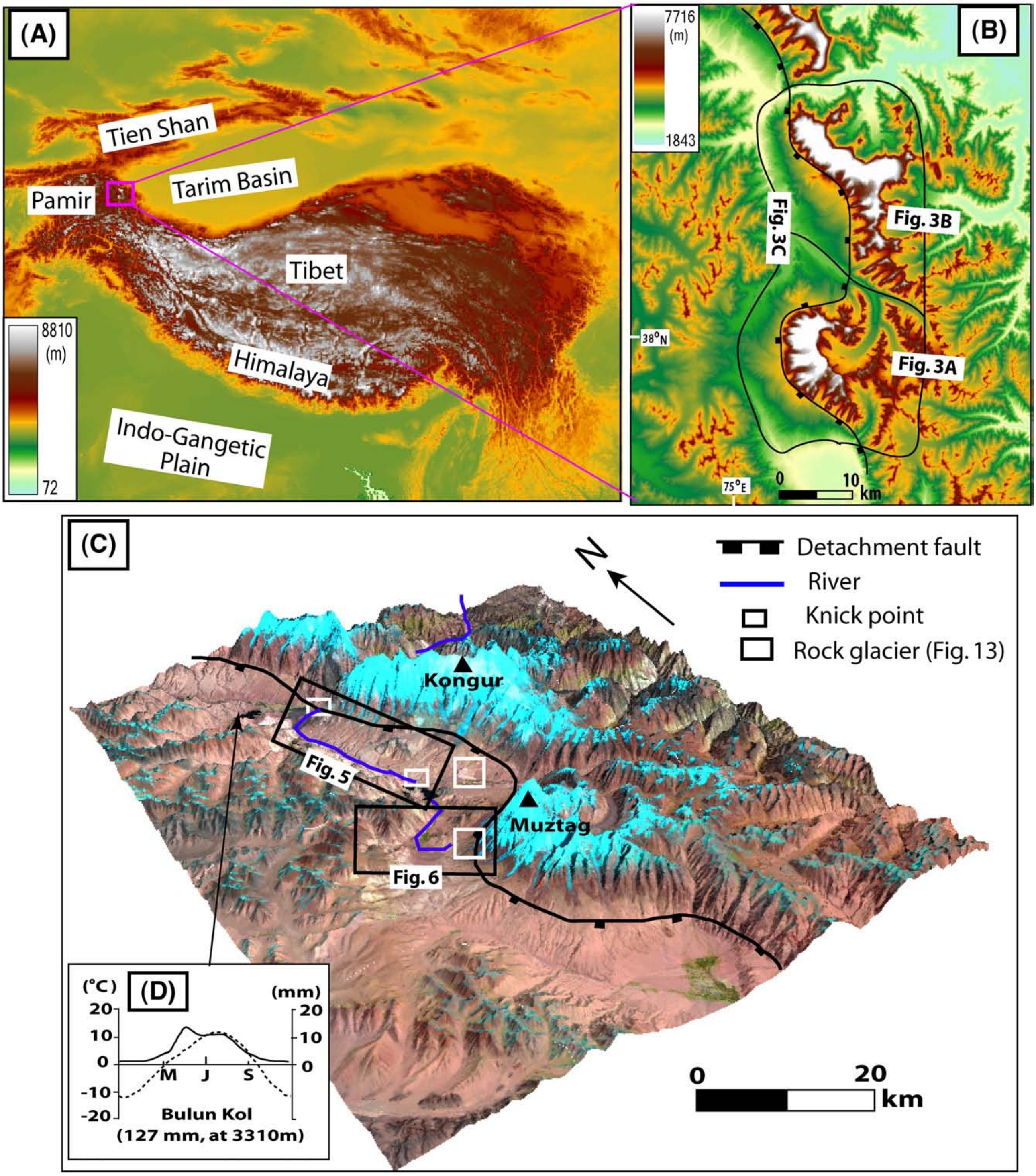

Fig. 2. The topography of the Tibetan Plateau (A) and the study area — Muztag Ata and Kongur Shan (B). Three dimensional view of study area showing the topography of the Muztag Ata–Kongur Shan (C). Kongur detachment fault runs from southeast to northwest. The inset (D) shows temperature (dotted curve) and precipitation (solid curve) of Bulun Kol, one of the villages located in the study region. Two knick points in the longitudinal profile of Kengxuwar River (Fig. 15) are marked as smaller boxes. The locations of rock glaciers in Fig. 13 are shown as bigger boxes.

supplied by mid-latitude westerlies. The lack of marine salts in snow at Muztag Ata, which would originate from moisture transported northward from the Arabian Sea by the Indian summer monsoon, supports the view that the mid-latitude westerlies provide the main source for present-day precipitation (Aizen et al., 2001).

Numerous authors have suggested that glaciers in this region are likely to be more sensitive to change in precipitation than temperature changes (Derbyshire, 1981; Shi, 2002; Owen et al., 2005). This characteristic may extend back beyond the last glacial cycle. In addition, the rapid exhumation that the region experienced over the last 2 Ma (Arnaud et al., 1993) probably changed the elevation and, therefore, the amount of precipitation supplied to and across this region. This in turn would have affected erosion on and around the massifs throughout the Quaternary.

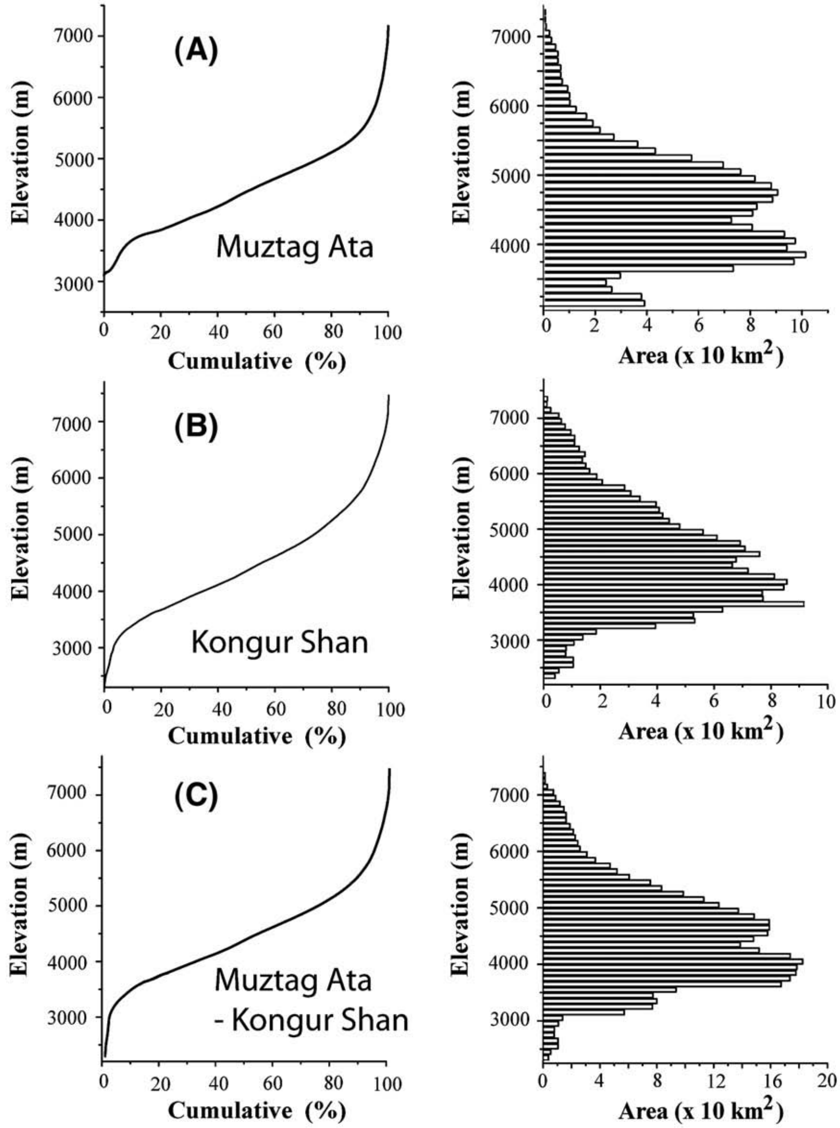

Fig. 3. Hypsometry curves and histograms showing the distribution of altitudes for Muztag Ata (A), for Kongur Shan (B), and for the whole study area of Muztag Ata and Kongur Shan (C). The boundary of each area is shown in Fig. 2B.

Impressive landforms, present within the valleys and intermontane basins of Muztag Ata and Kongur Shan, include scree cones, debris flow fans, moraines, glaciofluvial outwash terraces, alluvial fans and floodplains. Many of these landforms have been intensely eroded by fluvial processes, and the surfaces have been modified by debris flows and other slope processes.

The region is extensively glaciated; >60% of the land area is glaciated or is covered with glacial sediments (Fig. 4). Glacial geologic evidence shows that Muztag Ata and Kongur Shan have experienced at least three major glaciations and at least 10 smaller glacial advances (Seong et al., 2007; Table 1). The best evidence for these glaciations is found in the Kartamak and Olimde valleys. Seong et al. (2007) assigned these deposits to three glacial stages. The oldest and most extensive glaciation, the Karasu glacial stage, was characterized by highly degraded and denuded till benches containing scattered surface boulders that were deposited by an expanded ice cap. The second oldest glaciation, the Subaxh glacial stage, was of piedmont type of glacier. This produced hummocky moraines that comprise large boulders, many of which are intensely weathered. The most recent glaciation, the Olimde Glaciation, was a series of valley glaciations that incised deeply into the former glacial surfaces to leave multiple sets of sharp crested, latero-frontal moraines.

Seong et al. (2007) hypothesized that the change in style of glaciers in Muztag Ata and Kongur Shan might be caused by a significant reduction of moisture flux to the region. This possibly reflects a change in regional climatic forcing that might be the result of the progressive surface uplift of the Himalayan ranges on the south and/or the Pamir and the Karakoram to the west, which progressively restricted the supply of moisture by the Indian summer monsoon and the westerlies after they uplifted.

The region is dominated by two vegetation zones — alpine meadow and alpine tundra. The alpine meadow zone consists mainly of short grasses near lakes and ponds, and alpine tundra, dominated by moss and lichen, on the snow-free surfaces. Heavy summer grazing in the meadow zone has resulted in the vegetation which superficially appears more like a dry steppe biome.

3. Methods

We used 1:100,000 scale topographic maps of this region (Lanzhou Institute of Glaciology and Geocryology, 1994) help to locate study

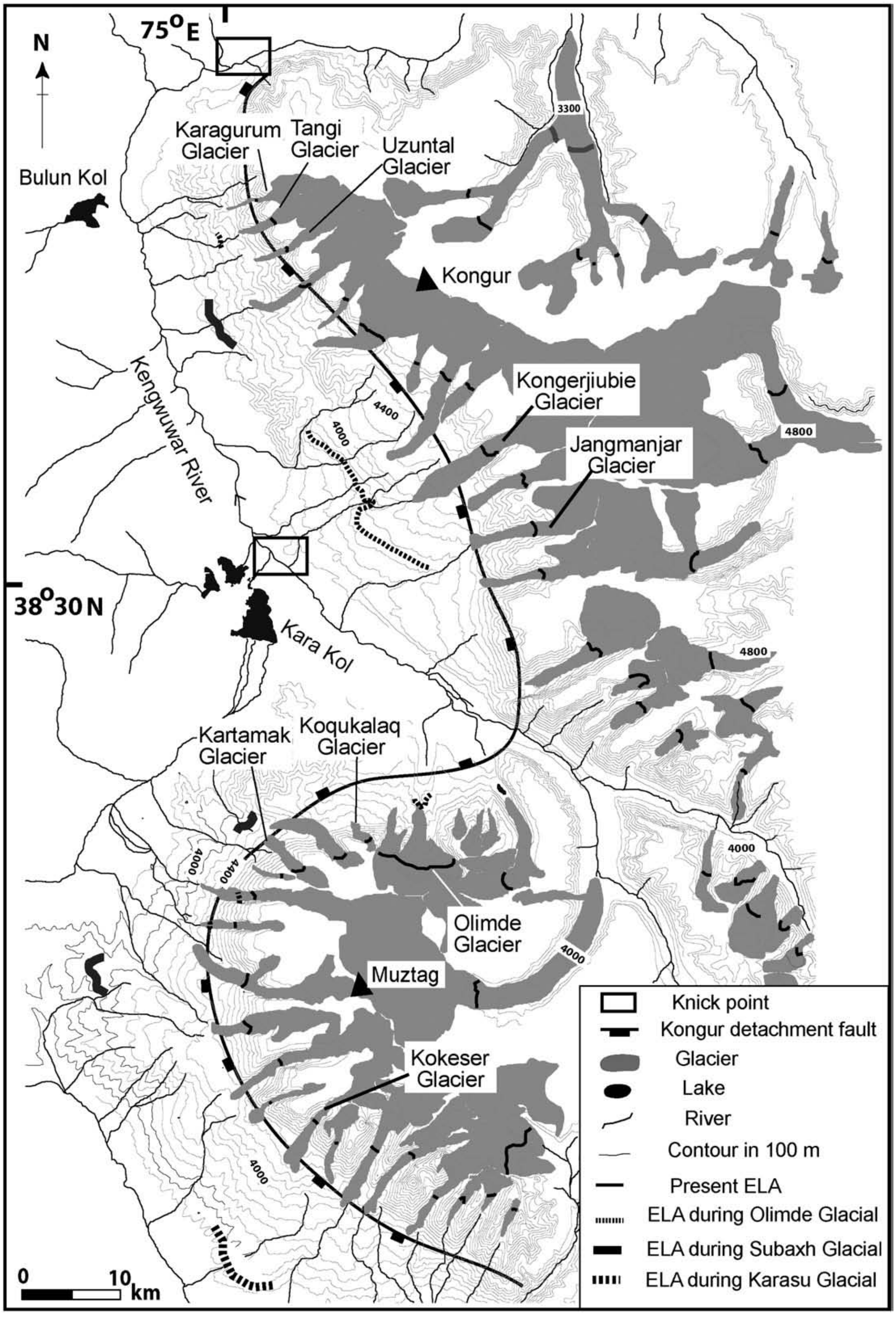

Fig. 4. Equilibrium line altitudes (ELAs) for the present and the last three glacial stages (see Fig. 2 for location). To calculate the former ELAs, only an accumulation area ratio of 0.67 was used for ease and for comparison with other regions.

areas. No detailed topographic maps are available and, therefore, detailed base maps were constructed with the aid of a hand held global positioning system (GPS) and satellite images, which included Enhanced Thematic Mapper Plus (ETM+; p150r33 and p150r34, respectively) and Advanced Spaceborne Thermal Emission and Reflection (ASTER) images (scene #: AST_L1A.003:2003030305 for Kongur Shan and AST_L1A.003:2003030307 for Muztag Ata). ASTER images, with 15 m horizontal resolution, have stereo sub-images for the construction of Digital Elevation Models (DEMs). The constructed DEM was used to help calculate present and past equilibrium line altitudes (ELAs), and to calculate a basin-averaged production rate for cosmogenic samples. Simplified versions of these geomorphic maps

Table 1
Summary of past glaciation around Muztag Ata and Kongur Shan (after Seong et al., 2007)

	Timing	Style	Likely prevailing moisture source
Olimde Glacial	Lateglacial and Holocene	Valley	Mid-latitude westerlies
Subaxh Glacial	Last glacial	Piedmont	Indian summer monsoon and Mid-latitude westerlies (?)
Karasu Glacial	Penultimate glacial	Ice cap	Indian summer monsoon (?)

are shown in Figs. 5 and 6. The area of landform types within both mountains was calculated from these maps and the DEMs (Fig. 7).

3.1. Digital Elevation Model (DEM)

A DEM provides topographic information and enables the modeling of surface forms. DEMs also are an important tool for the analysis of glaciers and glaciated terrains (Duncan et al., 1998; Bishop et al., 2001; Kääb et al., 2002). We, therefore, utilized ASTER data, which provides 14 bands of data at three resolutions, to develop a DEM. We used simultaneous stereo images of Visible and Near-Infrared (VNIR) nadir (3N) and backward (3B) to generate DEMs for this study. Scenes captured in September and October 2000 (cloud cover 5%) were used to generate absolute DEMs. The Geomatica 8.2 package from PCI Geomatics was used for the DEM extraction. An automated image-matching procedure was used to generate the DEM through a comparison of the respective gray values of these images with the help of the 1:100,000 scale topographic map. Thirty five and thirty two ground control points (GCPs), respectively, for each scene were collected and used to calculate the altitude. In addition, as many as 20 well distinguished locations (e.g. bridges, peaks, villages and roads) were employed as tie points (TPs) for better matching of two stereo images (3N and 3B). The resultant absolute DEM has a horizontal resolution of 30 m. Small holes because of cloud-cover were replaced using corrected-SRTM (Shuttle Radar Topography Mission) values. Finally, the two scenes covering the research area were stitched together using the same software that was used to generate the DEMs.

3.2. Equilibrium line altitude (ELA)

Comparisons between former and present equilibrium-line altitudes (ELAs) have yielded valuable information on climatic gradients and the magnitude and extent of climate change in the mountain areas (Ohmura et al., 1992;Benn and Lehmkuhl, 2000; Benn et al., 2005; Owen and Benn, 2005). ELAs were, therefore, determined to help quantify past and present glacial conditions in the Muztag Ata–Kongur Shan region. The geometric calculations for ELA reconstruction were made using the ASTER DEM (resolution 30 m) and the SRTM imagery (resolution 90 m). Glacial landforms were identified using ASTER and ETM+ satellite images. For modern glaciers, steady-state ELAs should ideally be based on observations of glacier mass balance over several years. Because of the lack of mass balance data, however, other multiple methods were used, which include the change of the shape of the convex direction of contour lines across glaciers on topographic maps, the hypsometric curve, a toe to headwall altitude ratio of 0.5 (THAR), the maximum elevation of lateral moraines (MELM), accumulation area ratios of 0.44 and 0.67 (AAR) and a balance ratio of 2.0 (BR). To calculate the former ELA, only an accumulation area ratio (AAR) of 0.67 was used. This was chosen to be comparable with published results for other regions (cf. Owen and Benn, 2005).

3.3. Terrestrial cosmogenic nuclide (TCN)

Two kinds of samples were collected to help determine the rates of erosion on bedrock and the massifs. Three bedrock samples (ME-15, ME-19, and ME-19-1) were taken from the top 5 cm surface of schist on bedrock knobs within the central valley. No evidence exists for erosion by glaciers. In addition, 17 samples of sand-sized sediments were taken from active stream beds.

All samples were prepared in the geochronology laboratories at the University of Cincinnati. First, the samples were crushed and sieved. Quartz was then separated from the 250–500 μm size fraction using the methods of Kohl & Nishiizumi (1992). After addition of ^{9}Be carrier, Be was separated and purified by ion exchange chromatography and precipitated at pH>7. The hydroxides were oxidized by ignition in quartz crucibles. BeO was mixed with Nb metal and loaded onto targets for the determination of the ^{10}Be/^{9}Be ratio by accelerator mass spectrometry at the Center for Accelerator Mass Spectrometry in the Lawrence Livermore National Laboratory. Isotope ratios were compared to ICN Pharmaceutical, Incorporated ^{10}Be standards prepared by K. Nishiizumi (Nishiizumi et al., in press) and using a ^{10}Be half-life of 1.5×10^{6} yr. The measured isotope ratios were converted to TCN concentrations in quartz using the total ^{10}Be in the samples and the sample weights. TCN ^{10}Be concentrations were then converted to steady-state erosion rate using a sea level high latitude (SLHL) ^{10}Be production rate of 4.98 atom per gram of quartz per year (Lal, 1991; Stone, 2000). Scaling factors were applied to compensate for altitude-dependent effect in calculating cosmic ray exposure ages (Stone, 1999). The error range for the converted rate of erosion is shown as one standard deviation (e.g. 10 m Ma^{-1}±1 σ).

4. Topography

The topography of the Muztag Ata–Kongur region can be divided into three zones (Fig. 3). The DEM shows that more than 80% of a land area lies between 3300 to 6000 m asl, which represents only 30% of the total relative relief (Fig. 3C), whereas the upper and lower components comprise only a small fraction of the surface area. The lower zone, below 3300 m asl, is coincident with most of the fluvial zone, and consists of the gorges and the over deepened valley floors of the rivers. The third zone lies at the highest altitudes and consists of the tallest ridges and peaks above 6000 m. The middle zone

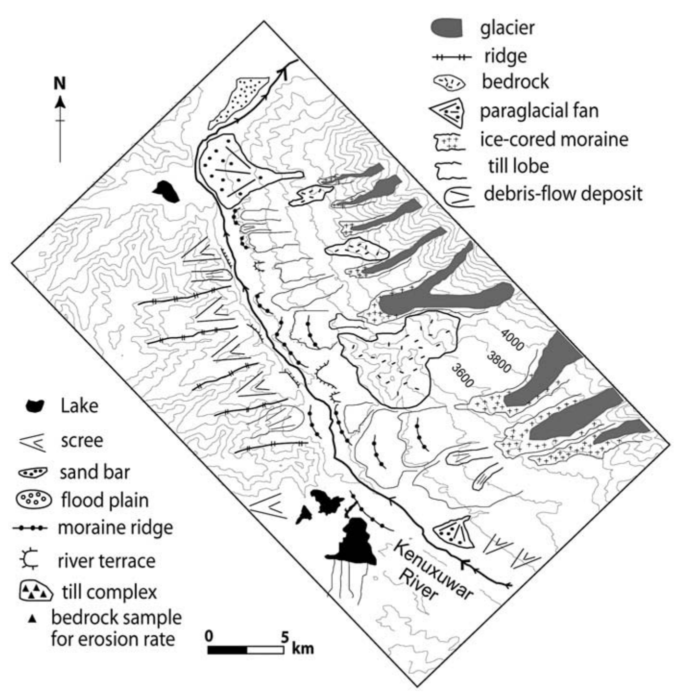

Fig. 5. Geomorphic map of Kengxuwar river valley to the west of Kongur Shan.

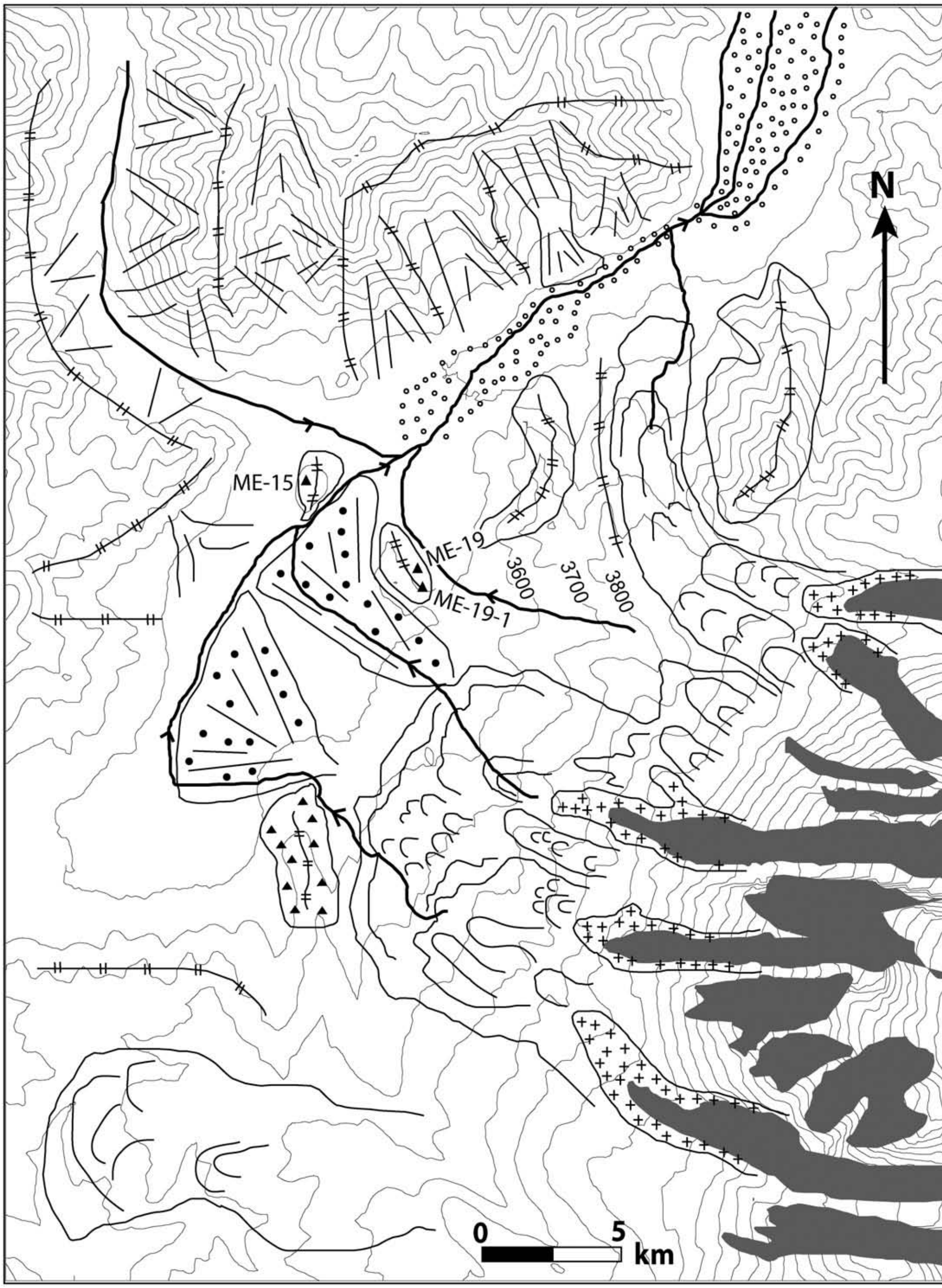

Fig. 6. Geomorphological map of Muztag Ata (see Fig. 5 for the legend and Fig. 2 for location). The locations of the bedrock samples for rates of erosion are shown in the center of the figure.

between 3300 m and 6000 m asl contains most of the mountain ridges and the glaciated surfaces. The two sectors with the highest frequencies in the histogram of elevation distribution for the total area are between 4400 and 4800 m asl and between 3500 and 4100 m asl (Fig. 3C). These altitude zones are coincident with the locations of the most extensive glacial deposits produced by the former glaciations. Two strikingly flat surfaces are present within the middle zone at the southwestern sector of Muztag Ata (Fig. 3C). These are areas where the deposits from a former piedmont glacier and rock avalanches are present.

5. Landforms

5.1. Glaciers and glacial landforms

Little previous work has been undertaken on the glaciers of the Muztag Ata–Kongur Shan region (Skrine, 1925; Fort and Peulvast, 1995; Ono et al., 1997) although recent studies have been conducted on similar glaciers in the Tadjik Pamir to the west (Zech et al., 2005). Most of the present-day glaciers are of high activity type (Andrews, 1975) with high altitude source areas and steep gradients. These

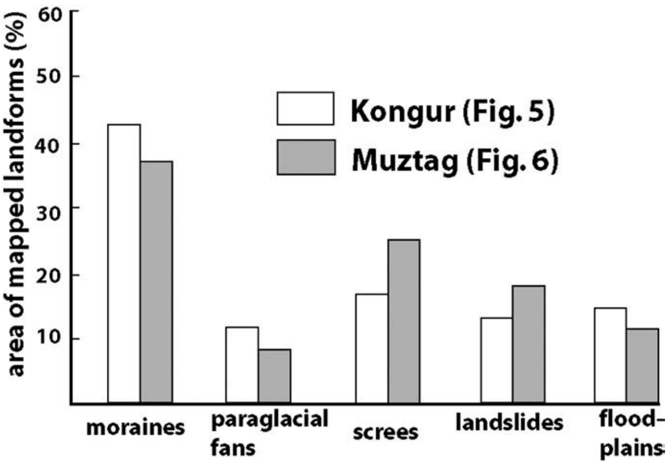

Fig. 7. Graph of the percentage of landform types for Muztag Ata and Kongur Shan.

glaciers are fed by direct snowfall and snow avalanching from the steep slopes. In many glaciers, the ablation areas are separated from source areas by steep ice falls or avalanche tracks. As a result, the snouts and ablation zones of many glacier are mantled by extensive and thick (>1 m) covers of angular debris containing boulders that exceed many meters in diameter (Fig. 8). Concentrations of sub-angular and edge-rounded clasts also occur on some glacier surfaces. These are probably the result of bands of subglacially transported debris that have been elevated to the surface of the ice. The amount of debris transported through subglacial process, however, has yet to be quantified.

Thick-debris covered glaciers are present on the east side of both massifs. The debris on the glacier greatly reduces ablation of underlying ice, and in some cases has resulted in the isolation of debris-covered ice masses from more rapidly-melting clean ice up-valley. In Himalayan environments, thick debris cover reduces sediment transfer by the glacier through a reduction in glacier velocity and ultimately can result in the formation of a rock glacier (Owen and England, 1998; Shroder et al., 2000). Ablation in debris-covered areas is focused on locations where bare ice is exposed, particularly in areas where debris has slumped and exposed bare ice. This is common around moulins and crevasses. Ablation proceeds by backwasting of ice cliffs and in some cases, produces chains of temporary thaw lakes on the glacier surface (Fig. 9A). The ultimate depositional product of this process is a drape of hummocky moraine usually between 5 and 10 m thick (Fig. 9B).

In contrast, many of the smaller glaciers devoid of debris are most common on the western slopes of Muztag Ata. The ablation zones of these glaciers comprise impressive ice pinnacles and supraglacial channels down which shallow supraglacial water flows (Fig. 10). Supraglacial streams, however, are spotted and intermittent and, thus, sublimation is likely important for the ablation of many of these glaciers.

Impressive sets of latero-frontal moraines occur down valley of the margins of most glaciers (Fig. 11). The tills have crude internal bedding that dips away from the former glacier margins. This reflects successive mass movements (particularly slides and flows) from the former glacier surfaces, in combination with intermittent glacio-fluvial reworking. A section in till on the west of Muztag Ata provides an example of the sedimentology produced by this process (Fig. 12).

The form and sedimentology of many moraines are similar to those of the Pasu-type glacial landform association described by Owen and Derbyshire (1989) in the Karakoram Mountains, although thick-debris covered glaciers on the eastern sides of both massifs are more similar to Ghulkin-type glaciers (Figs. 11 and 12). The Kartamak glacier (Fig. 10) typifies the glaciers in the Muztag Ata–Kongur region. It has small hummocky moraines and parallel ridges comprising a terminal moraine. Thin (<3 m thick) subglacial lodgement tills are present and form on the sides of bedrock knolls, or roche moutonnées. The relative low gradient and topography of the forelands of the glaciers are probably responsible for controlling the formation of Pasu-type. Ghulkin-type glacier landform associations, however, are also present (Fig. 11). Of note are the Uzuntal and Tangi glaciers, which have well-developed latero-frontal moraines surrounding the snouts similar to Ghulkin-type glacier landform associations. The Uzuntal Glacier (Fig. 11B) has a thick frontal moraine ~15 m high and with ~30 ° slopes, while the Tangi Glacier (on the right side in Fig. 11A) has a

Fig. 8. View looking west of Karayaylak glacier from the lateral moraine (38°42.554′ N, 75°16.820′ E) formed during Little Ice Age showing the supraglacial debris and striking lateral moraines.

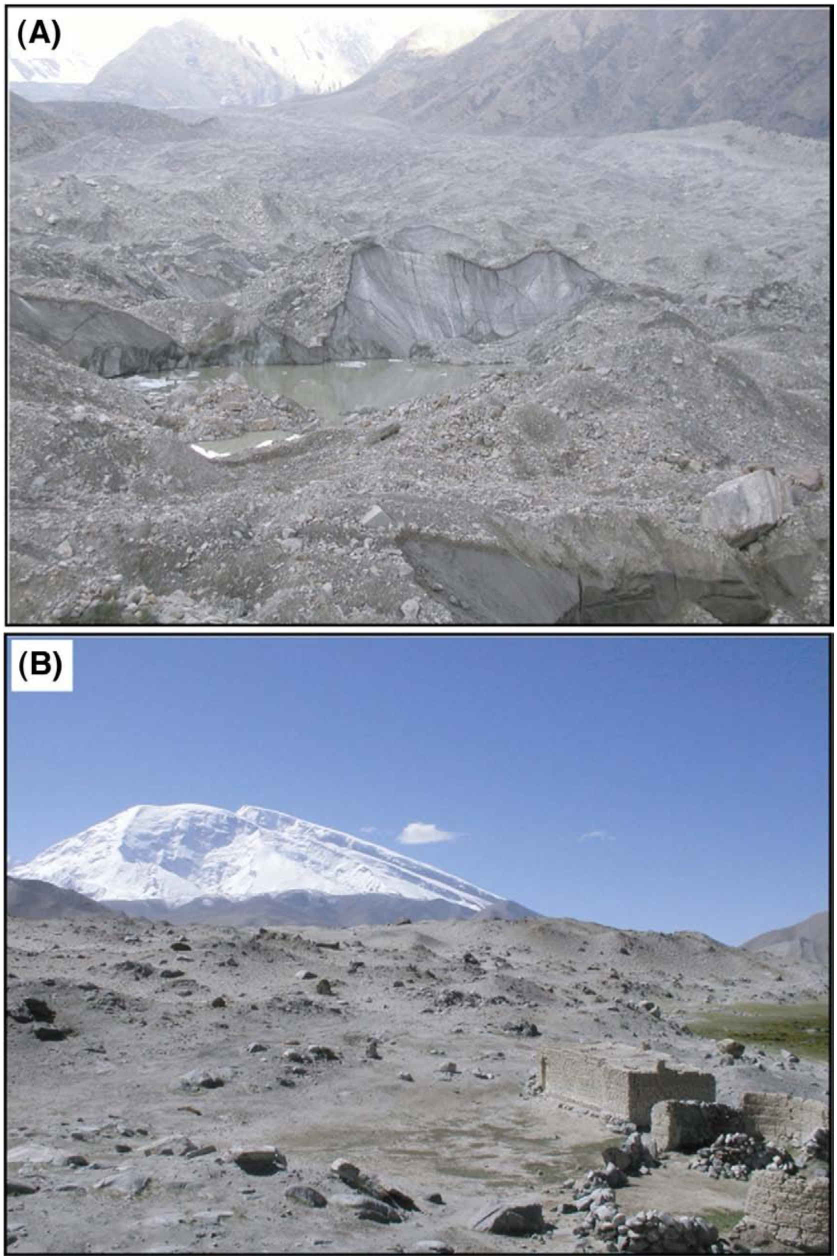

Fig. 9. Glacier landform in the Muztag Ata–Kongur Shan region. (A) View looking east of thaw lakes developed on Karayaylak glacier by surface ablation and backwasting. (B) View looking east of hummocky moraine. The peak in the left background is Muztag–Ata dome at 7715 m.

~60 m high lateral moraine. Its terminal moraine formed ~2000 years ago (Seong et al., 2007). Because of extensive ablation, the right portion of the frontal moraine of Uzuntal glacier is mantled by supraglacial debris and has become a rock glaciers. Unlike the typical Ghulkin-type glaciers, these examples have not developed ice-contact fans because of limited glacio-fluvial action.

Seong et al. (2007) noted that the extent of glaciation has decreased with time, from ice caps to piedmont glaciers to valley and cirque glaciers. Likewise, the dominant type of glacial landform has changed with time from Ghulkin-type to Pasu-type landform associations. The glacial landforms produced during the penultimate glaciation are similar to Ghulkin-type landform associations, characterized by thick ice-contact fans. In contrast, landforms produced during the Last Glacial and the Holocene are more similar to the Pasu-type glacial landform associations, typified by chaotic hummocky moraines and small terminal moraines ridges.

5.2. Rock glaciers

Glaciers at the western end of the Himalayan–Tibetan orogen have highly variable debris-loads with varying efficiencies of sediment transfer from the accumulation zones to the termini (Owen and Derbyshire, 1989; Bishop et al., 1995). Many of these glaciers have debris concentrations that are so high that they are on the verge of becoming rock glaciers. Owen and England (1998) described examples of such glaciers, which had become rock glaciers in the Karakoram Mountains of northern Pakistan.

In the Muztag Ata–Kongur Shan region, active and relict rock glaciers occur in many valleys in association with the contemporary glaciers. Active forms are particularly abundant on west-facing slopes of both massifs, where they descend to 4000 m asl. These are complex and in places override older fossilized rock glaciers and debris flow fans (Figs. 13A and 14A). The successive development of these rock glaciers

Fig. 10. View of the terminus of less debris-covered glacier. The person on the snout provides a scale.

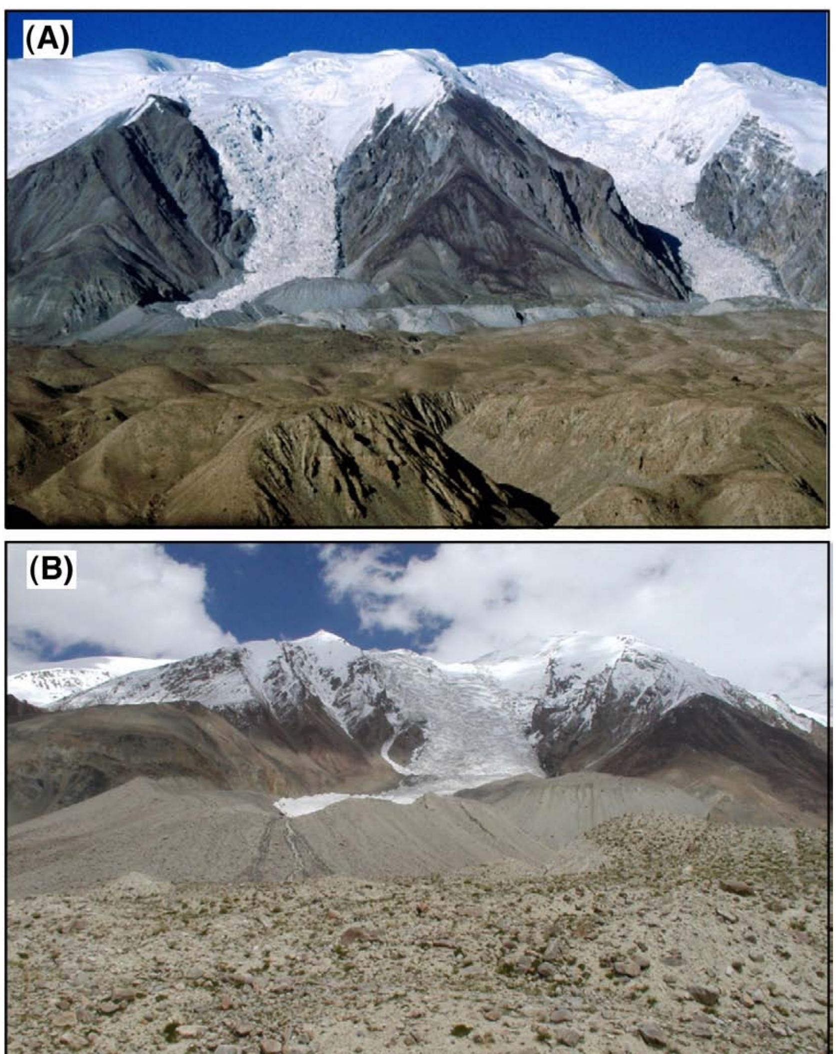

Fig. 11. Ghulkin-type of glaciers. (A) The Uzuntal glacier with it thick latero-frontal moraine is located to the left and Tangi glacier with a thick long latero-frontal moraine (right) and (B) view of Uzuntal glacier. The frontal moraine rises ~15 m high.

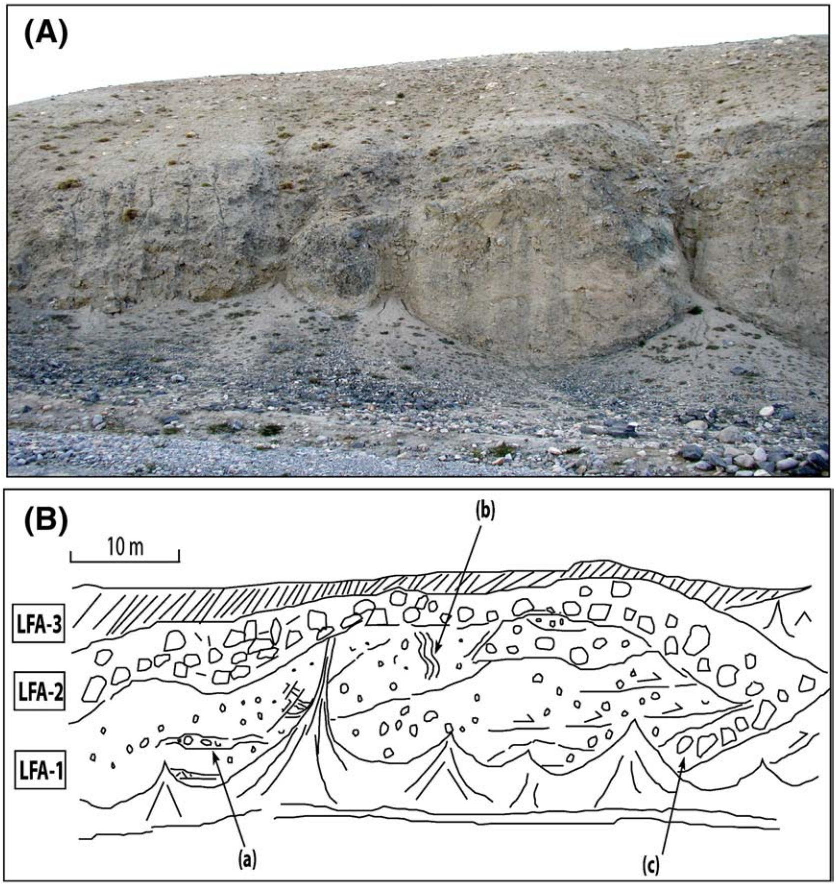

Fig. 12. Till complex found ~700 m downvalley from the Kartamak Glacier (A) and its interpretation (B). Lithofacies association 1 (LFA-1) is massive pebble to cobble diamict with open framework (a) and reworked structure (b) related to subglacial process. LFA 2 is massive boulder diamict with jigsaw structure and ghost clasts (c), indicating the boulders fell on the glacier, and LFA 3 is scree deposited by mass movement.

results in a complex assemblage of lobes, which define areas of differential movement. Scree cones and slopes provide additional sediment input into many of these rock glaciers, which descend as a complex assemblage of lobes and shear zones and reflect differential movement of debris lobes. The surface of the rock glaciers is commonly stepped with a number of lateral ridges, which display compressive folds in the lower reaches, as well as lateral shears along the margins where boulders are vertically oriented. The lobe fronts (Figs. 13B and 14B) form slopes up to 30 m high, with angles up to 50 . These are subject to frequent collapse by mass movement processes, such as debris flows, avalanching and rock sliding, which result in rapid advance of rock glaciers and transport of sediment. The rock glaciers shown in Fig. 13 originate along the snout of thinning, debris mantled glaciers.

Protalus rock glaciers (Fig. 14C) are also present in Muztag Ata, but development is restricted to altitudes of between 3500 and 4000 m asl on south-facing slopes. They occur on slopes with angles between 15 and 20°, and are restricted to surfaces that have unconsolidated slope deposits. These are characterized by multiple arrays of lobate ridges that have a relief of between 0.5 and 1.0 m high. Owen and England (1998) described similar forms in the Karakoram Mountains and Himalaya to the south of Muztag Ata and Kongur Shan.

5.3. Rivers

The rivers in this region are dominated by glacier meltwater, although snow melt and direct precipitation also contributes to the hydrology. As such, the Kengxuwar River, a trunk river in this region, is characterized by large diurnal and seasonal variations in discharge. Most of precipitation is supplied from March to May as snow, which does not melt until the summer. Thus, the stream discharge of tributary rivers on the west slope of Muztag Ata is small except during the summer ablation season when meltwaters from snow patches and glaciers drain into the rivers.

The Kengxuwar River is the main stream (with a Strahler stream order (1952) of 4 derived from a 1:100,000 scale map) that drains the Muztag Ata–Kongur Shan massifs. Its tributary channels, draining glaciers to the east, connect to the Kengxuwar River as it skirts along the eastern margin of Muztag Ata and Kongur Shan and then along the northern margin of Kongur Shan, ultimately flowing northeast through the high mountains and into the Tarim Basin. The river channels are dominantly braided, comprising cobbly and pebbly bars and swales, which are modified seasonally because of the high variability of discharge.

The longitudinal profile of Kengxuwar River, from its origin at the Kartamak glacier on the west-facing slope of Muztag Ata toward the Tarim Basin, is shown in Fig. 15. Two knickpoints are apparent. The first occurs at the gorge running from the moraine-dammed lake (Kara Kol) through hummocky moraine while the other is present just beyond the junction of Gez River and Kengxuwar River, in which the river crosses the Kongur detachment fault.

5.4. Lakes

The largest lake in the region, Kara Kol, is over 3 km long and occupies a bowl-shaped basin that is blocked by hummocky moraines that formed during the early Holocene (Seong et al., 2007). Smaller lakes occur on glaciers, for example, a small lake is present on the debris-mantled Karayaylak glacier (Fig. 9A). Structurally controlled lakes are also present including the large, shallow lake at Bulun Kol (Fig. 4) that formed as a result of subsidence of the hangingwall along the Kongur detachment fault (Fig. 2C).

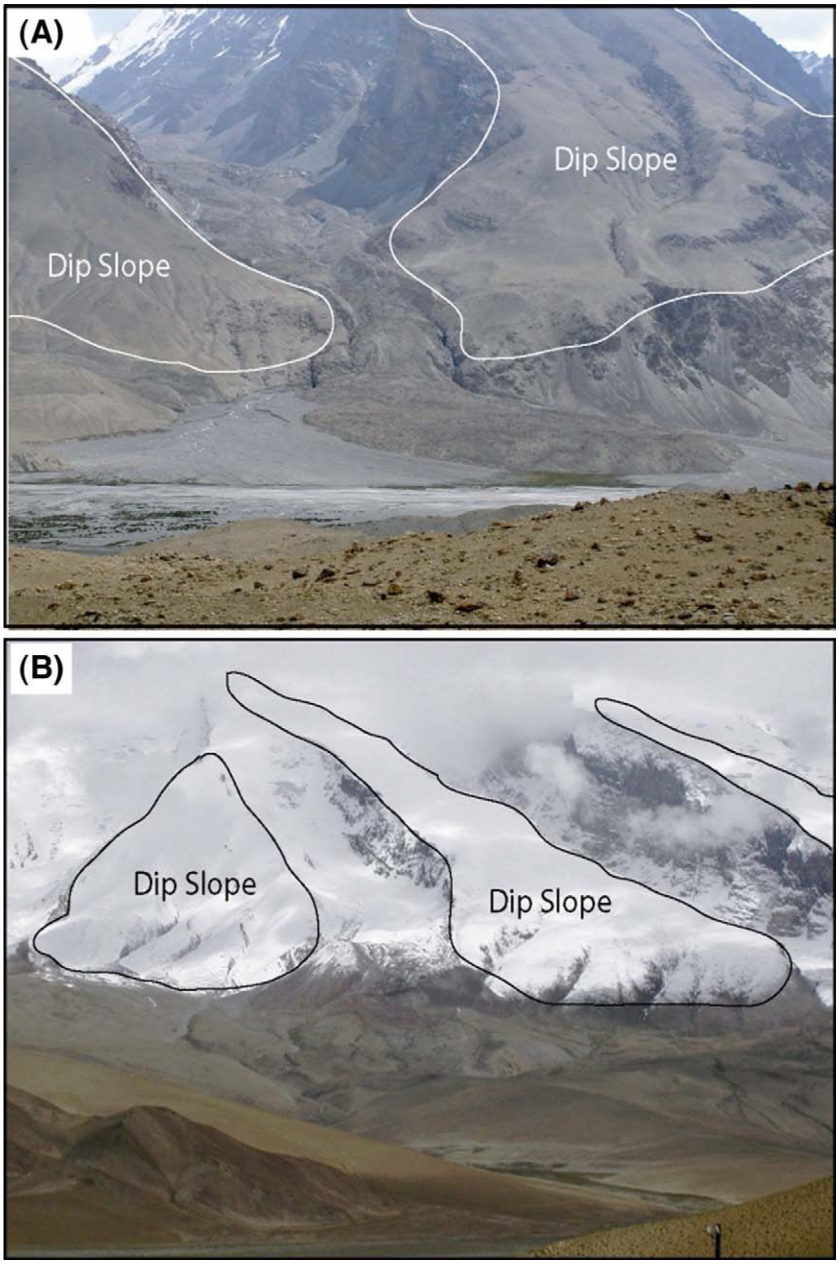

Fig. 13. Selected rock glaciers on Kongur Shan (A) view of rock glacier on Kongur Shan, looking north from the terminal moraine (38°21.819′ N, 75°10.239′ E) below Olimde glacier. The width is ~3 km and (B) view looking east of rock glacier on Muztag Ata. Width of rock glacier is >2 km.

5.5. Alluvial and outwash fans

Alluvial and outwash fans are present throughout the lowest altitudinal zone. The alluvial and outwash fans are typically steep (5–10°) and radiate from the glaciers, from eroded moraines and from incised terraces. The fans comprise meter thick beds that dip sub-parallel to the surface of the fans composed of cobbles and pebbles and are occasionally interbedded with pebbly sands.

The alluvial fans in the lower valley of the Karagarum glacier (Fig. 16) are an excellent example of such landforms. The source valley has a distinctive morphology, comprising a steep (15–20°) upper erosional slope that contains narrow gullies cut into a moraine ramp and a deep gullied channel down which sediment is transferred. Boulder clusters are present within the main channel and silt to pebble size material is common along the channel floors. The present channel has shifted to the south, compared with the axis of the fan. The lower depositional zone of the fan is characterized by its gentle (5–7°) slopes and planar surfaces. The surface of the fan can be differentiated into different sub-areas on the basis of weathering and rock varnish development. The deposits on the fan comprise decimeter beds of matrix-supported cobbles and pebbles. The beds dip sub-parallel to the surface of the fan.

5.6. Terraces

The terraces throughout the region comprise dominantly glacial, fluvial/glaciofluvial and lacustrine sediments. The best developed and exposed terraces are present along the Kengxuwar River (Figs. 17 and 18). These comprise fluvial/glaciofluvial sediments (LFA-1) that are overlain by lacustrine sand and silt (LFA-2) or are capped by glacial sediments (LFA-3). The fluvial/glaciofluvial sediments comprise decimeter and meter beds of poorly sorted sands and gravels, which are occasionally imbricated. The glacial sediments are massive matrix-supported diamicts that contain boulders and cobbles. The overlying

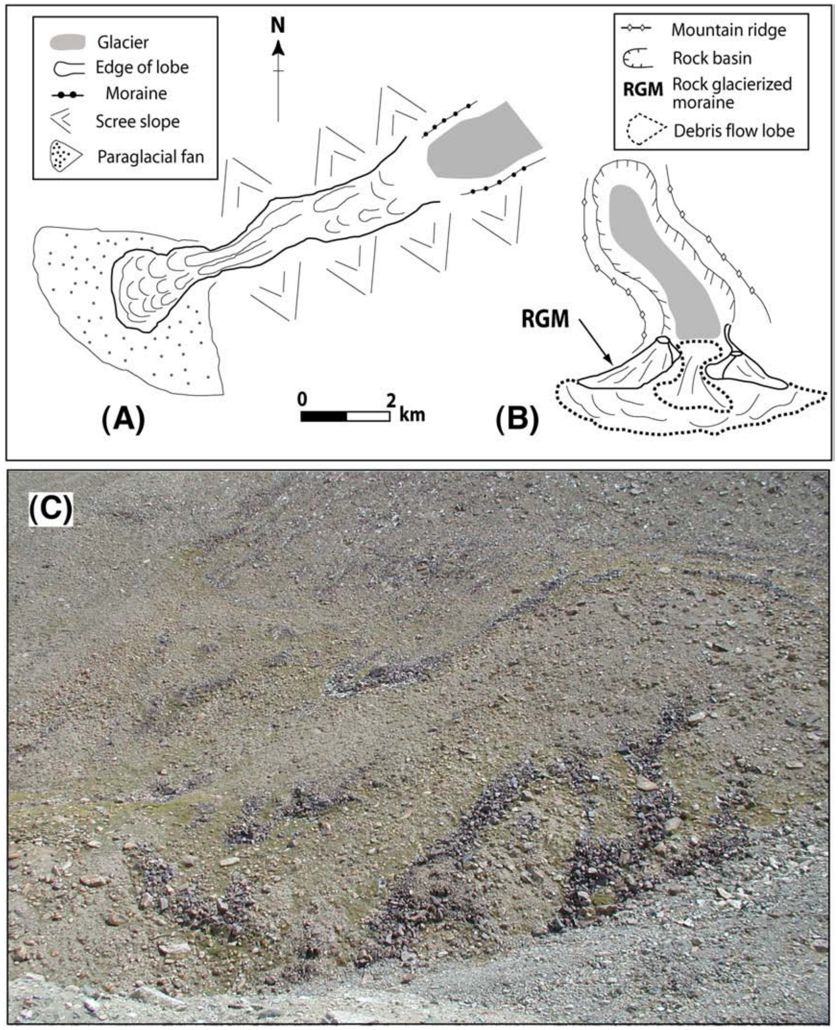

Fig. 14. Geomorphological maps of rock glaciers on Kongur Shan (A) and Muztag Ata (B) marked as a purple box in Fig. 2C and (C) view (38°21.620′ N, 75°10.101′ E) looking northwest of pro-talus rock glacier developed on the south wing of Muztag Ata. The field of view is ~200 m.

lacustrine sediments comprise light brown planar bedded silts and fine sands. Seong et al. (2007) dated one of these glacial terraces to ~ 50 ka using by TCN surface exposure dating.

5.7. Landslides

Deposits from mass movements are common throughout the region and are particularly prevalent in the middle and upper altitudinal zones. These include rock and debris falls, debris flow

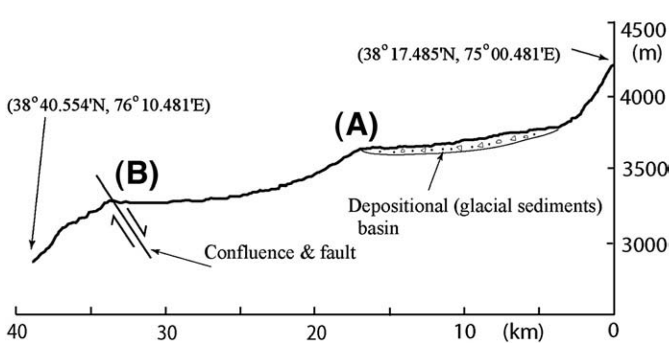

Fig. 15. Longitudinal profiles of Kengxuwar–Gez River system. (A) is just below the gorge of hummocky moraine that dams the lake (Kara Kol). (B) is beyond the junction of Kengxuwar and Gez rivers and Kongur detachment fault that crosses it.

and snow avalanche deposits. Long-runout landslides are also present throughout the region. Many of these may have been initiated by earthquakes. The Karakulun landslide, for example, was initiated by the Taghman earthquake (Fig. 19B). The most impressive long-runout landslide is present at Kokoser (Fig. 20), a 10 km wide, lobate deposit that slopes from the main fault scarp of the Kongur normal fault. The surface of the landslide deposit is a chaotic assembly of debris arranged in longitudinal ridges and groves that slightly diverge from the mountain front to form a fan-like pattern (Fig. 19B). The margin of the landslide deposit is steep (>30) and high (100 m). The most distal margin is banked against the eastern slopes of the opposite side of the valley. Sections through the termini of the Kokoser landslide deposit reveal a massive diamict containing angular clasts that reach several hundred-cubic-meters in size, which are supported in a matrix of silt and mud. Fort and Peulvast (1995) interpreted this deposit as an avalanche-debris flow. They considered its kettle-like surficial morphology as indicative of mass movement processes with debris incorporating rock and ice. Although its causal mechanism is not known, it is possible that an earthquake initiated the failure.

6. Erosion rates

The concentration of in-situ produced TCNs in sediment within a catchment area is inversely related to the rate of erosion of the

Fig. 16. View looking northeast from the road (38°38.379′ N, 74°58.003′ E) at the paraglacial fan developed down the snout of the Karagurum Glacier (Fig. 4).

catchment (Brown et al., 1995; Bierman and Steig, 1996; Granger et al., 1996). As a result, the TCN concentration in sediment will be lower in rapidly eroded catchments. Calculating rates of erosion for catchment areas that have been glaciated, however, is challenging because of the likelihood of considerable storage of sediment with moraines and/or terraces, together with sporadic transfer of sediment over the history

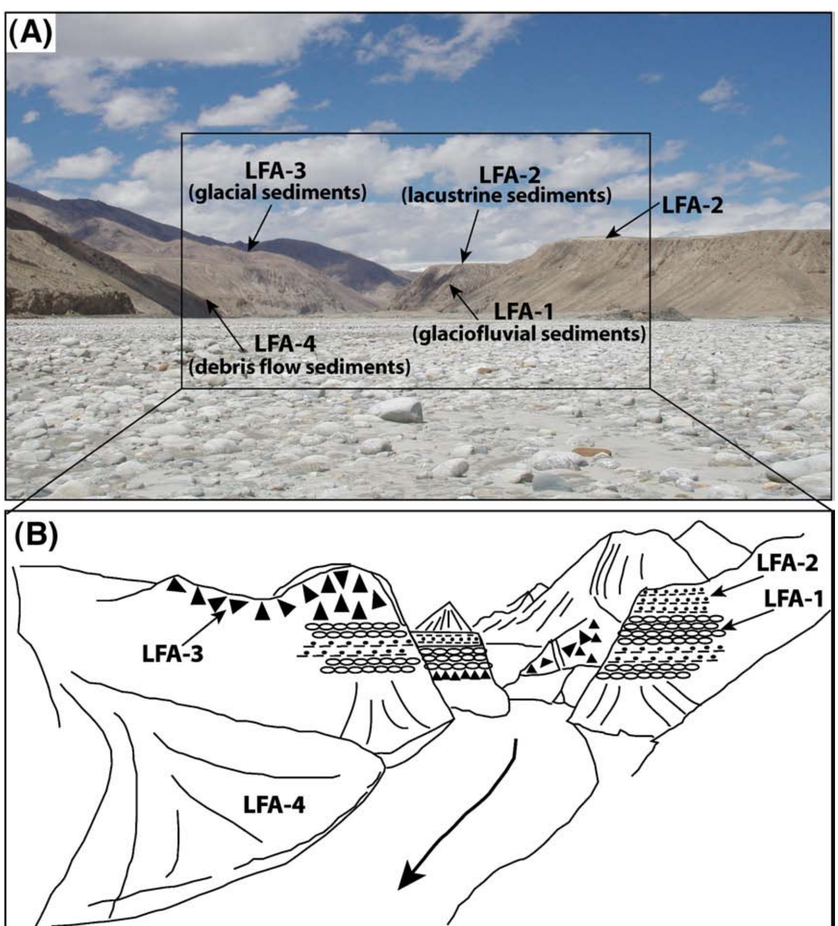

Fig. 17. Glacial, fluvial/glaciofluvial, and lacustrine sediments comprising the terraces along Kengxuwar River valley. Lithofacies association 1 (LFA-1) is glacio-fluvial gravel deposit, LFA-2 is lacustrine deposit consisting fine sand and silt, LFA-3 is boulder dominant till deposit, and LFA-4 is angular gravel and cobble dominant debris flow deposit.

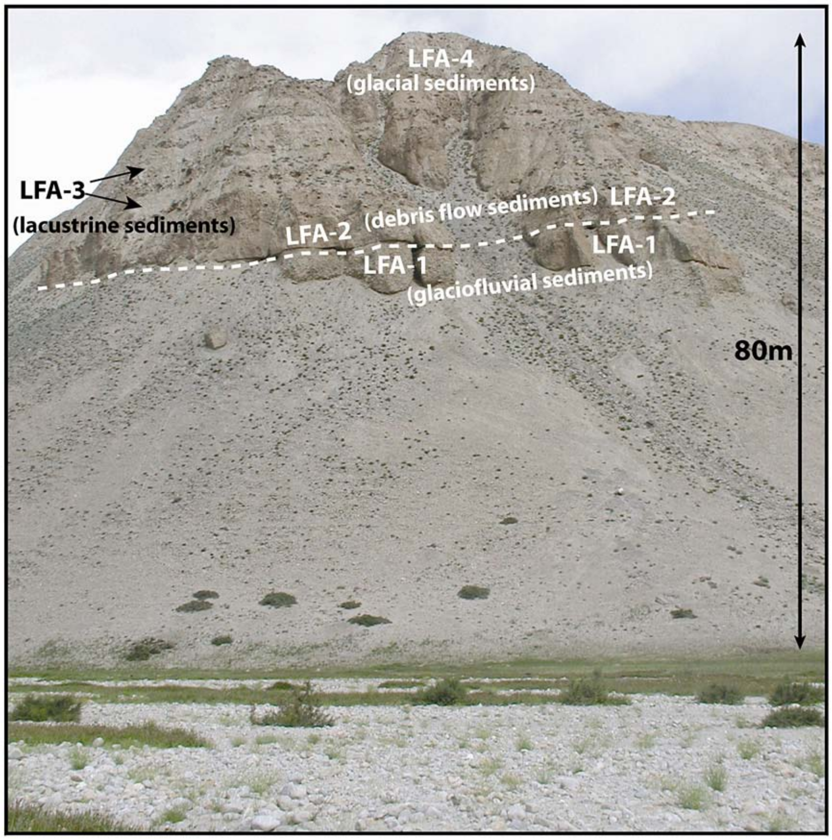

Fig. 18. View looking northeast from the present floodplain of Kengxuwar River (38°38.006`N, 74°58.125`E), showing boundaries among various doposits comprising terraces. LFA-1 (lithofacies association) is glacio-fluvial gravel deposit, LFA-2 is angular gravel and cobble dominant debris flow deposit, LFA-3 is lacustrine deposit consisting of fine sand silt, and LFA-4 is boulder dominant till deposit.

of the catchment. Furthermore, young, glaciated catchments likely provide overestimates of long-term erosion as substantial bedrock is removed during glacial times, which is rapidly transferred downstream and ultimately out of the catchment and essentially dilutes the TCN concentrations in sediment. Despite these caveats, TCN concentrations provide a proxy for examining regional validity and provide estimate for rates of erosion within glaciated catchments.

To calculate rates of erosion and sedimentation for selected catchments from TCN concentrations, catchment area-integrated nuclide production rates were calculated by combining catchment hypsometry (determined from the DEMs) and using the altitude production-rate function of Lal (1991) in 100 m bins (Fig. 21). Catchment-wide rates of erosion (Table 2) were calculated using the methods of Bierman and Steig (1996) and applying the following equation:

$$\varepsilon = \frac{\Lambda}{\rho}\left(\frac{P}{N} - \lambda\right) \quad (1)$$

where N is measured activity (atoms ^{10}Be g^{-1} quartz), P is basin integrated rate of production (atoms ^{10}Be g^{-1} quartz yr^{-1}), ε is the rate of erosion (cm yr^{-1}), ρ is density (g cm^{-3}), and Λ is attenuation depth (150 g cm^{-2}). Approximately 70% of the area in the catchments that were examined for erosion studies had slopes <20°. Moreover <5% of the area had slopes greater than 35°. Thus, consideration of slope effects on TCN production is small (less than a few percent of the total rates of production).

The ^{10}Be TCN concentrations in sediments and bedrocks, and calculated rates of erosion are shown in Table 2 and Fig. 21, respectively. The rate of erosion determined from the sediments collected from catchment areas that contain only Strahler (1952) 1st and 2nd order streams (as determined from the 1:100,000 scale map), range from 540 to 1400 m/Ma (ME-1 through ME-5, ME-9 and ME-10). These samples were collected along streams which incise Holocene and Late-glacial moraines. In contrast, rates of erosion for catchments that contain higher order streams range from 22 to 103 m/Ma (ME-6, ME-8, ME-11 through ME-14, ME-16, ME-18 and ME-20). These samples were collected from regions blanketed by older (pre-Late-glacial) moraines. Rates of bedrock erosion (ME-15, ME-19 and ME-19-1) are lower than the catchment area wide rates and range from 11 to 23 m/Ma (Fig. 22). The bedrock surfaces might have been covered by snow or regolith which reduced the TCN production. No evidence exists, however, that the bedrock surface was significantly covered. The TCN surface exposure ages of the bedrock surfaces is 30-50 ka. The sampled bedrock knobs may have been glaciated during the Karasu glacial stage (penultimate) and early Subaxh (MIS 3 or 4) glacial stage. Considerable variability occurs in the rates of erosion between adjacent samples determined for the 1st and 2nd order streams. For example, samples ME-2 through ME-5 have rates that range from 610 to 1402 m/Ma. The variation among adjacent samples for higher orderstreams is significantly less. Samples ME-12, ME-14, ME-17 and ME-18, for example, range from 67 to 103 m/Ma. Higher variability associated with the lower order streams likely reflects less effective mixing of catchment wide TCNs than that for the higher order streams.

7. Discussion

7.1. Geomorphic zones and glacier change

The landscape evolution of the Muztag Ata–Kongur Shan region has been strongly influenced by tectonics and fluctuating climate,

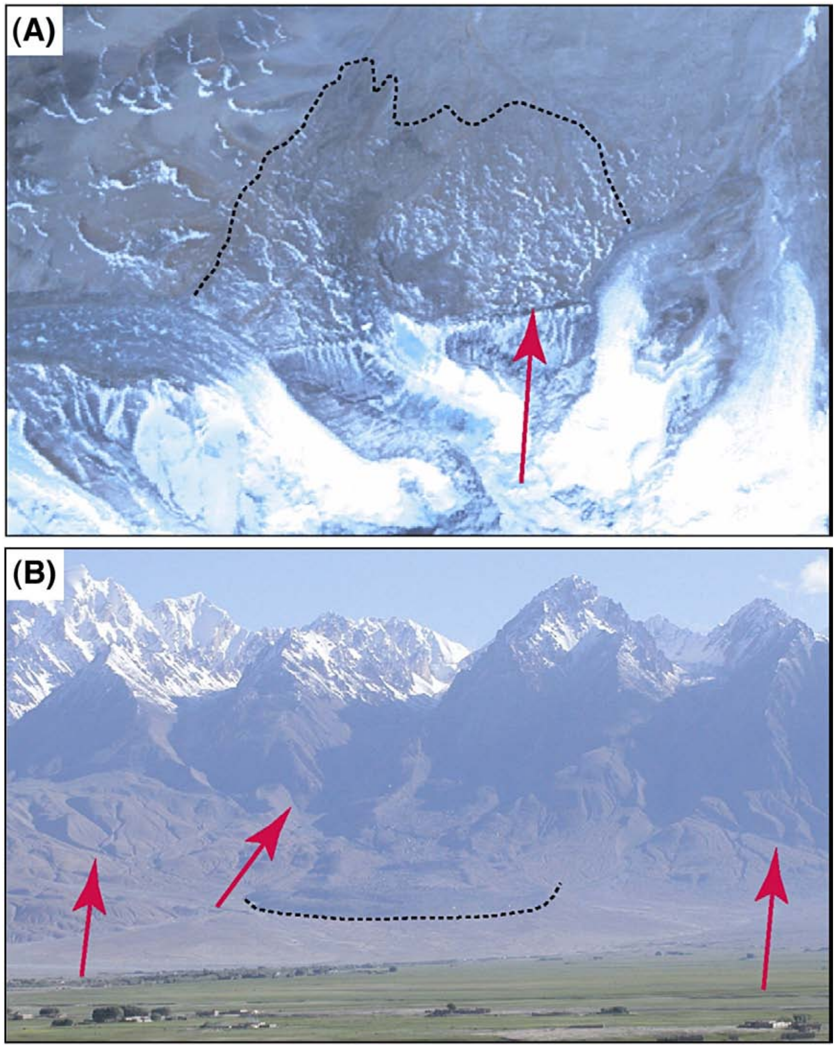

Fig. 19. (A) ASTER scene showing the surface rupture and landslide (dotted line) by earthquake around the snout of Koqukalaq glacier. (B) View looking northeast from the road (38°00.378′ N, 75°01.691′ E) of Karakulun landslide (dotted line) caused by Taghman earthquake. Multiple lines of strike–slip fault line (arrow) running from the southeast through to alluvial fans to the northwest. Both locations are marked as a purple box in Fig. 2C.

which in turn have controlled the magnitude and frequency of geomorphic processes within the region. Rapid tectonic uplift and exhumation together with intense glacial and fluvial incision have produced steep, long slopes. As a result, a clear altitudinal distribution of landforms occurs throughout this region. These can be broadly assigned to four zones (Fig. 23C). The relative importance of the geomorphic processes within the region can be largely assessed by comparing the aerial extent of landforms on Kongur Shan and Muztag Ata (Figs. 7 and 24).

The glacial stratigraphy and history of the region is described by Seong et al. (2007). They showed that the oldest glaciation, the Karasu glacial stage, was most extensive. During this glacial event, an expanded ice cap developed and filled the Kengxuwar valley to produce a thick and extensive succession of hummocky moraines. The following glaciation, the Subaxh glacial stage, however, resulted in the sediments in the Kengxuwar valley being intensely eroded and ultimately overlain by glaciofluvial sediments. Glaciers continued to oscillate throughout the Holocene, the most extensive of these advance occurred at ~8 ka (Seong et al., 2007). This advance blocked the Kengxuwar River and left a moraine-dammed lake (Kara Kol in Fig. 4). Substantial quantities of sediments were transported out of the mountains via the Kengxuwar River system during these times, and produced deeply incised glacial valleys and transported sediment to the Tarim Basin. The present depositional landforms, such as bars, and low terraces in the channel, therefore, probably serve as relatively short-lived storage.

The changing style of glaciation over the last few glacial cycles is intriguing. Each successive glaciation has decreased in extent; from mountain ice caps to piedmont glaciers to valley glaciers. The decrease in extent of glaciation through time can be also recognized in the surrounding mountains of the Tibetan Plateau (Owen et al., 2006) and other areas, including Tasmania, the Sierra Nevada, Alaska, Peruvian Andes, Patagonia, and Chilean Lake District (Denton et al., 1999; Barrows et al., 2002; Smith et al., 2002; Kaufman et al., 2004; Singer et al., 2004). Thus, glaciers in high mountains might have decreased in extent over time, because of compensating growth of the Northern Hemisphere ice sheets over the last several glacial cycles. The decreasing extent of glaciation in this particular setting, however, possibly also reflects a change in regional climatic forcing that resulted from surface uplift of the Karakoram and Himalayan ranges to the south and the Pamir to the west, which progressively restricted the supply of moisture by the monsoon and mid-latitude westerlies (Seong et al., 2007). Alternatively, the progressive uplift of the massif and its feedback on deep incision of its valley might have had a topographic control on the style of glaciation, and resulted in glaciers that had less extensive catchments and were confined to deep valleys.

Reconstruction of former glaciers allows changes in ELAs to be determined for the region. The present and former ELAs are shown in

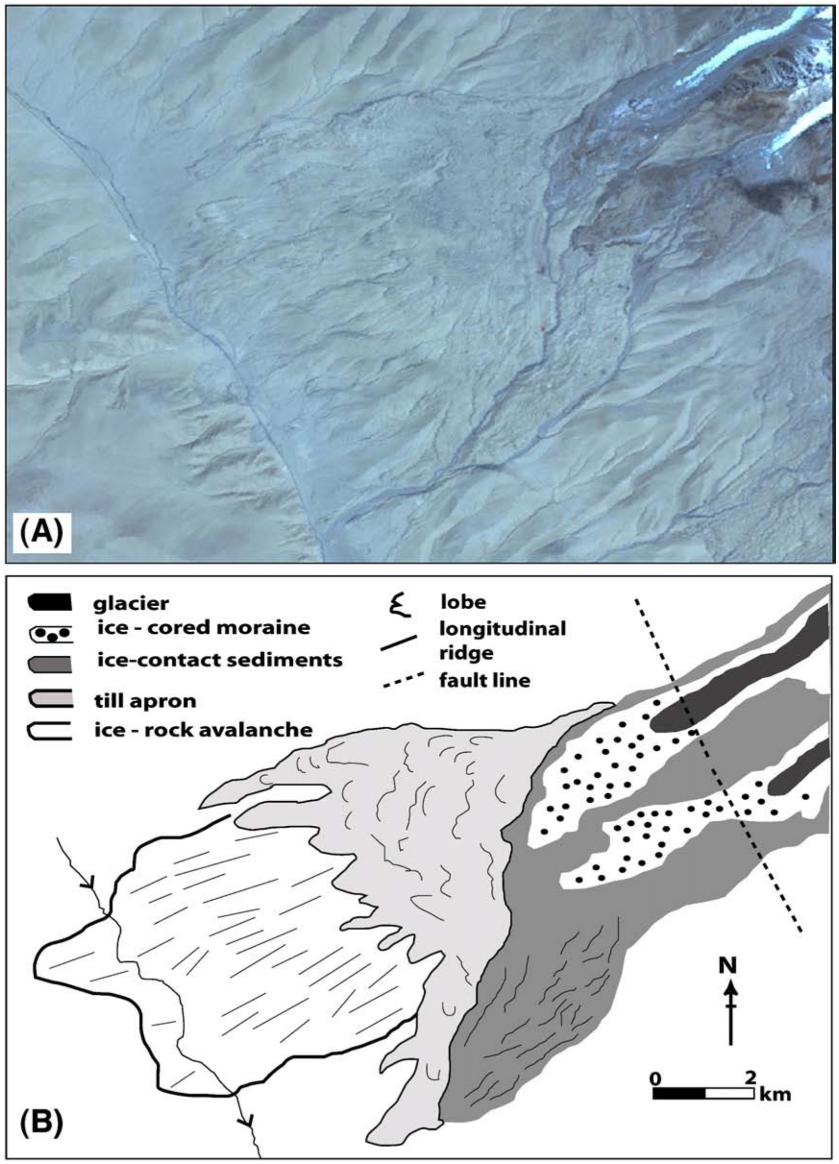

Fig. 20. False-color ASTER Image of Kokoser landslide deposit (A) and its interpretation (B; modified from Fort and Peulvast, 1995).

Fig. 4 and Table 3. The thick debris covered glaciers have the lowest ELAs in the region and are as much as 1500 m lower in elevation than the cleaner cirque glaciers. As suggested by Ono et al. (1997), the ELAs on the west (Tibetan) side are up to 1000 m higher than the east (Tarim Basin) side. If the thick, long debris covered glaciers on the east side are excluded from the calculation, however, the present ELA of the clean, valley glaciers on the west side are actually on average 30 m lower than the east side, suggesting an orographic precipitation effect from westerly sources. The lower ELA on the east side of the range when debris mantled glaciers are considered likely results from the difference in topography and its consequence of supraglacial debris cover. The eastern side with its steep slope is more susceptible to snow avalanching, resulting in the increase in supraglacial debris mantle and, thus, mass balance onto the glacier.

During the Karasu glacial stage, the expansion of the extent of glacier ice caused all the tributary glaciers above 3400 m asl to coalesce. An average ELA depression (ΔELA) of 1975 m has been calculated for this glacial stage on the west side of the range. During the Subaxh glacial stage, the average ΔELA was 1350 m on the west. During Olimde glacial stage, the glaciers were likely supplied moisture from mid-latitude westerlies and advanced multiple times in phase with north Atlantic climate deterioration (Seong et al., 2007). The average ΔELAs were <600 m, except for a glacial advance at ~8 ka (ΔELA of >1300 m), which was almost as great as the ΔELA during the Subaxh glacial stage.

Among the well dated glacial successions in the Himalayan–Tibetan orogen, the upper Hunza Valley in the Karakoram Mountains and the Khumbu Himal are the only regions were a ΔELA for the global LGM has been adequately determined (Owen and Benn, 2005). These regions show that the ELA descended by <300 m during the global last glacial maximum. Unfortunately, no moraines exist in the Muztag Ata and Kongur Shan area that have been dated to the global LGM. The ΔELAs shortly after LGM in this region, however, were between 300 and 400 m. This is comparable and consistent with values in the Hunza Valley and Khumbu Himal.

7.2. Topographic asymmetry and glacial buzz-saw model

The marked E–W precipitation gradient across the region likely influences the distribution of topography, glaciers and landforms. The western sides of the massifs, for example, are situated on the wetter upwind side of the mid-latitude westerlies, where westerly

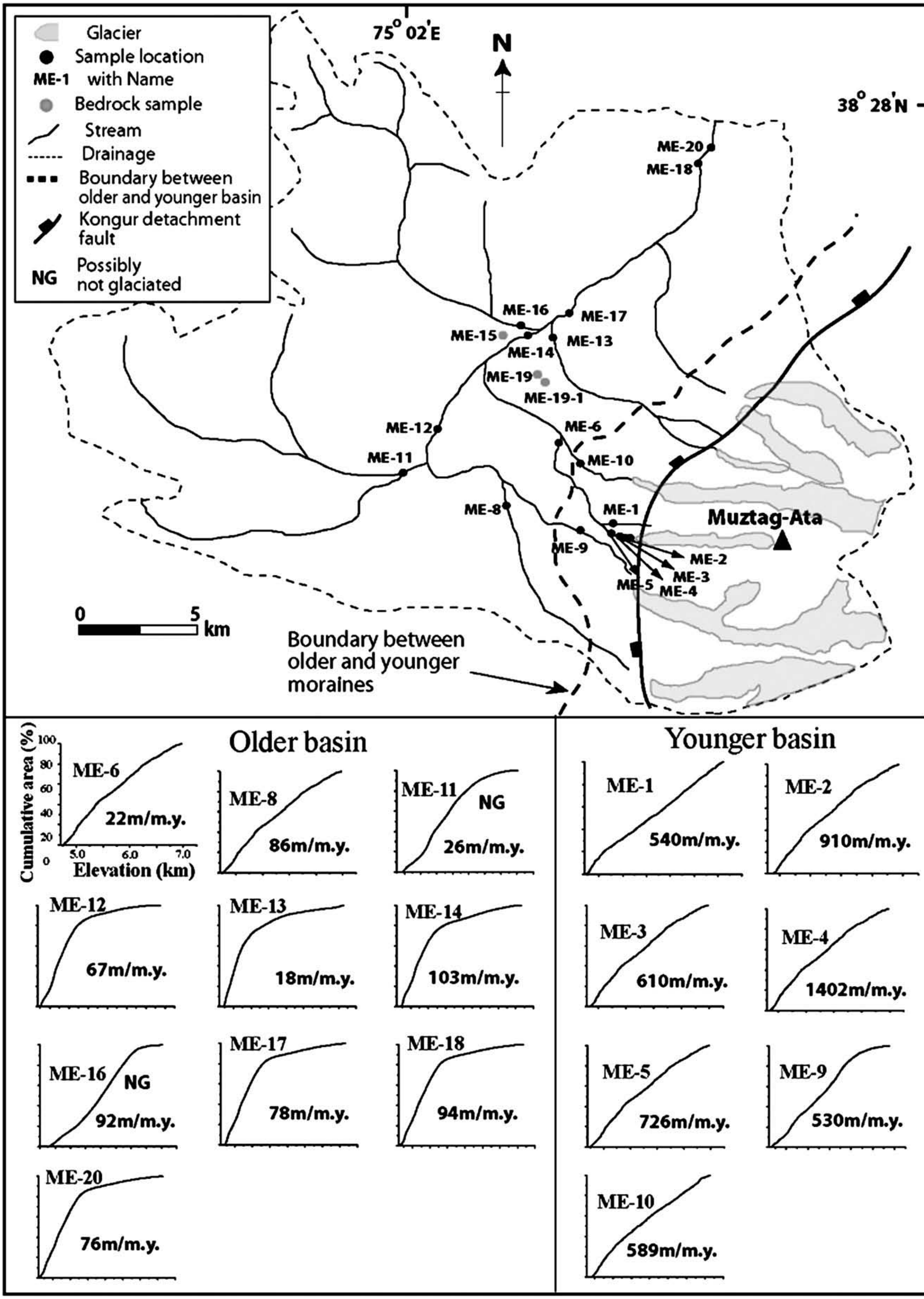

Fig. 21. Cosmogenic sampling sites for basin-wide rates of erosion and bedrock (ME-15, ME-19, and ME1-19-1). Hypsometric curve of each sampling site for calculation of basin-wide rate of cosmogenic production in Table 3.

Table 2
Rates of erosion of basin and bedrock from cosmogenic ^{10}Be

Sample	Latitude (±0.001 N)	Longitude (±0.001 E)	Altitude (m asl)	^{10}Be (10^6 aoms/g)	Erosion rate (m/myr)	Drainage Area (km^2)	^{10}Be production Rate (atoms g^{-1} a^{-1})
ME-1	38.291	75.008	4209	0.09±0.01	540±36	6.02	80.71
ME-2	38.285	75.012	4293	0.06±0.01	910±34	5.31	84.13
ME-3	38.286	75.012	4287	0.08±0.01	610±45	5.89	83.87
ME-4	38.287	75.009	4232	0.04±0.01	1402±54	6.05	81.60
ME-5	38.287	75.004	4181	0.07±0.01	726±44	6.27	79.53
ME-6	38.315	74.977	3852	1.85±0.04	22±9	17.13	67.11
ME-8	38.302	74.965	3878	0.48±0.02	86±23	33.12	68.03
ME-9	38.304	74.963	3855	0.08±0.01	530±37	25.58	67.21
ME-10	38.321	74.986	3858	0.07±0.01	589±41	12.82	67.32
ME-11	38.360	75.005	3742	1.46±0.04	26±10	116.97	63.29
ME-12	38.321	74.939	3807	0.59±0.02	67±22	209.03	65.52
ME-13	38.336	74.989	3828	2.27±0.07	18±6	19.83	66.26
ME-14	38.354	74.973	3749	0.37±0.02	103±25	306.53	63.53
ME-15	38.336	74.983	3896	3.66±0.09	15±1.2	Bedrock	
ME-16	38.357	74.983	3753	0.42±0.01	92±13	86.45	63.66
ME-17	38.383	75.008	3699	0.48±0.02	78±11	427.54	61.84
ME-18	38.420	75.050	3651	0.39±0.01	94±13	535.20	60.25
ME-19	38.354	74.962	3910	1.72±0.05	23±1.6	Bedrock	
ME-19-1	38.354	74.962	3908	3.64±0.11	11±0.9	Bedrock	
ME-20	38.460	75.053	3663	0.48±0.02	76±	550.67	60.65

precipitation resulted in small, clean valley glaciers during multiple Holocene advances. In contrast, the eastern slopes, are on the drier leeward side of the mid-latitude westerlies, contain clean cirque glaciers with a higher average ELA than the valley glaciers on the west side of the divide. A few large debris-covered glaciers, however, are also present with extremely steep headwalls. These lower the average ELA of the east side of the divide significantly. Snow avalanching and rock falls from the high peaks to the lee sides of the massifs likely increased the mass balance and debris supply to produce the long debris-mantled glaciers.

The asymmetry of the massifs, which is well illustrated by the DEMs (Fig. 24), is likely the consequence of the faulting and uplift. Because exhumation is oblique, a dip-slope, exhumed fault surface is exposed on the west flank, and erosion is limited to valleys inset into the fault surface (Fig. 13). It may be difficult for large glaciers to take root on the sloping surface. On the east side of the divide, concentrated glacial erosion, dominated by the few, large, debris-mantled glaciers, has likely removed significantly more material. Large glaciers are fed by avalanche and rock fall from the peaks which surround them. Concentrated glacial erosion probably contributes to uplift by denudational unloading in the footwall of the Kongur detachment and/or the subsidence of the hanging wall initiated or accelerated by thick sediment loading. This effect may be enhanced by inefficient fluvial evacuation of the hanging wall basin, which is evidenced by the lower rates of erosion measured in the hanging wall basin over the last 10^3–10^5 yr, compared to the long-term (>10^6 yr) rates of exhumation of the detachment footwall.

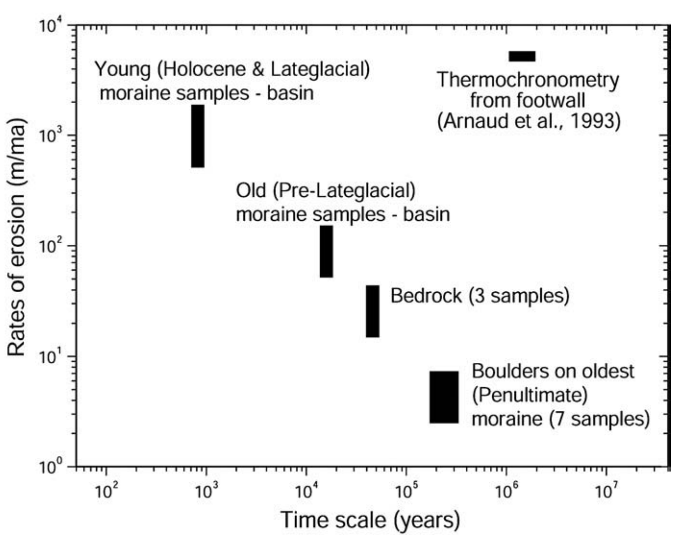

Fig. 22. The comparison of rates of erosion among different time scales. Each box delimit ranges of measurements and corresponding time scales, for cosmogenic nuclides, which average over thousands of years or ~60 cm of erosion, and for thermochronometry (^{40}Ar/^{39}Ar ages and K-feldspar diffusion modeling) data (Arnaud et al., 1993), which average over tens of millions of years or 3.6 km.

The control of climate on the topography via the glacial system can be illustrated by comparing the western and eastern sides of the massif. The western/windward side shows the highest peak around former ELA between 3700 and 4200 m asl. The hypsometry for the eastern/lee slopes, however, has the dominant zone around the present ELA of the cirque glaciers between 4700 and 5200 m asl (Fig. 24). Furthermore, the mean elevation of western windward side (4371 m asl) is lower than the lee side (4845 m asl). The contrasting results of the asymmetry might result from the development of the long, thick debris covered glaciers on the lee side, which have lowest ELA but relatively smaller contribution to the calculation of the area. Also, the east/lee side lies entirely within the footwall of the Kongur detachment, where relief is expected to be higher, whereas the west side of the range includes a thick, moraine mantled, relatively low-relief portion of the hanging wall as well, where elevations are lower.

The hypsometry for the whole region shows that highest altitude frequency is focused in two altitudinal zones, between 4400–4800 and 3500–4100 m asl. These altitudes are coincident with the ELAs for glacier during the Olimde glacial stage and Subaxh glacial stage, respectively (Table 3). This suggests that the topography of the region is largely controlled by glaciation (Porter, 1989) and glacial erosion is most efficient in the elevation range of the ELA (Andrews, 1972). Further, it is consistent with the glacial buzz-saw hypothesis, which argues that glaciers can act to erode the landscape to the level of the ELA, regardless of the rate uplift (Brozovich et al., 1997).

7.3. Paraglaciation

The geomorphic form and sedimentology of the fans and terraces in this region are typical of those described by Barnard et al. (2003, 2004a,b, 2006) that formed by resedimentation during deglaciation, and are, thus, described as paraglacial in origin. The abundance of these paraglacial landforms suggest that much of the landscape development in this region likely occurred during short periods of time as the landscape responded to oscillating glaciers. During the Holocene, as many as eight glacial advances occurred and it is likely

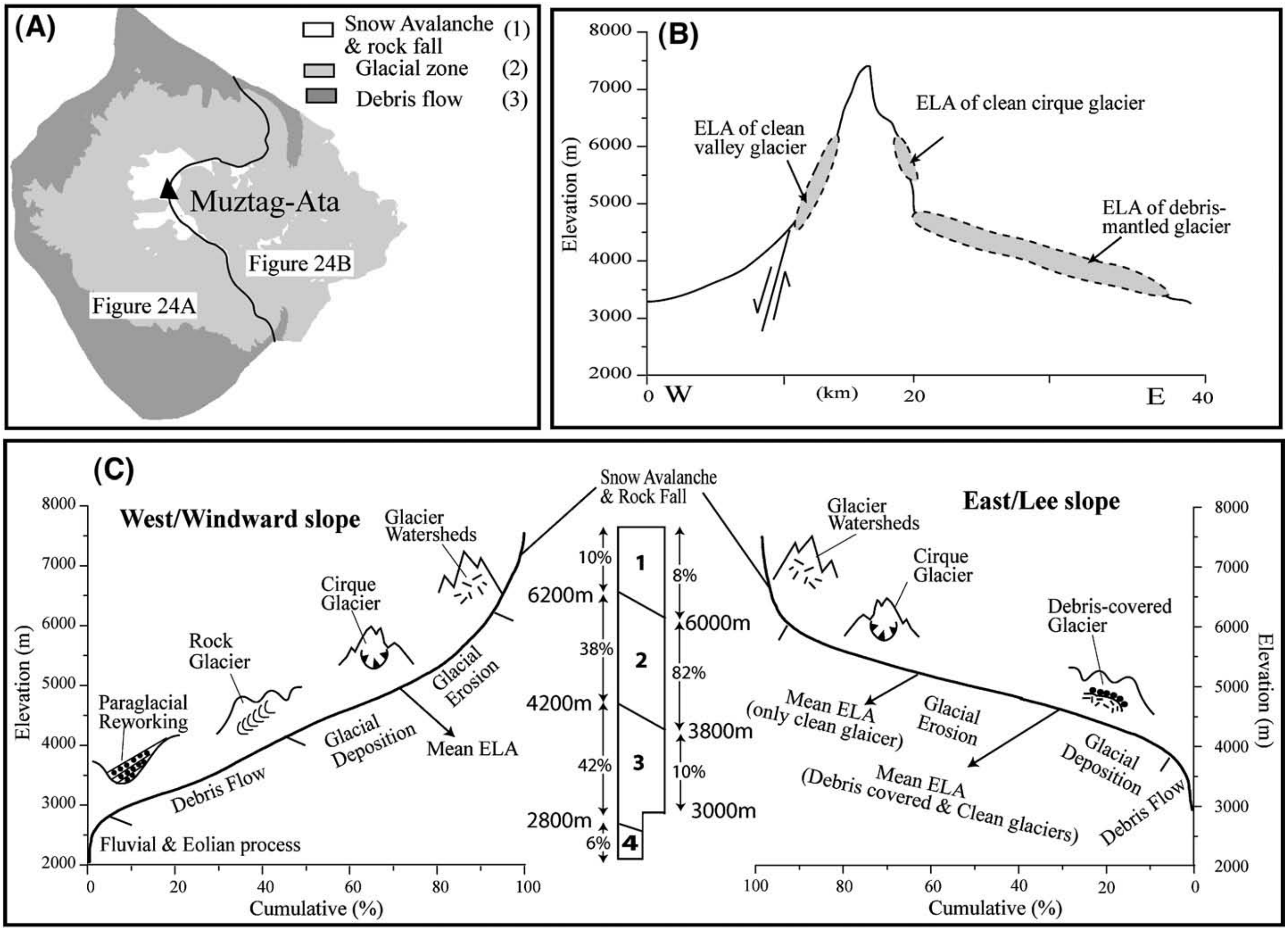

Fig. 23. The altitudinal zonation of dominant geomorphic processes across the high peaks of Muztag Ata (A) and the whole area (C). (1) The zone for snow avalanche and rock fall. (2) Glacial activity-dominant zone consisting of accumulation and ablation zone. (3) Debris flow (mostly paraglacial reworking)-dominant zone. (4) Fluvial and aeolian process-dominant zone. (B) The cross-section across Muztag Ata shows the contrasting ELA distribution.

that glaciers fluctuated considerably during the Pleistocene. Upon each glacial oscillation, the hydrologic system and associated processes, such as fluvial erosion and sedimentation and mass movement, would have been dramatically influenced. This would have resulted in oscillating sediment transfer and landform development.

As a combination of landscape readjustment during deglaciation and the high relief in the Muztag Ata–Kongur Shan region, the very susceptible unconsolidated glacigenic sediments are intensely reworked by non-glacial processes, resulting in rapid degradation of glacial landforms and release of large quantities of sediment into the fluvial system. The evolution of the valley reflects the dynamic relationship between glacial, slope and fluvial processes within and among the three altitudinal zones. A variety of slope processes contribute to debris transfer across this region, including, the falling, rolling, and sliding of clasts from the overlying slopes, debris flow and snow avalanching. Sediment is fed directly into the stream channels, occupied by steep and fast-flowing streams. Silt to cobble size sediment is quickly transferred along these streams, whereas bouldery deposits are commonly temporarily stored along the channels to be later removed during higher discharges during deglaciation or extreme events such as glacial lake outburst floods. Extreme paraglacial events can be identified by the thick bouldery diamicts and within channels and fan deposits (Fig. 16).

Most slopes show major modification by mass movement initiated by paraglacial processes. This is similar to neighboring mountains of the Karakoram and Himalaya, where landsliding is common and involves a variety and combination of processes, including falls, toppling, avalanching, sliding, and flows (Shroder et al., 1999; Barnard et al., 2001). As a consequence, paraglacial mass movements are common and are major slope forming processes (Fig. 7). The widespread distribution of alluvial fans in association with glaciated valleys is notable and suggests that mass movement is probably intensified following deglaciation, as large areas of unconsolidated debris are exposed on steep slopes. The suggestion is supported by higher rates of erosion of the samples collected proximal to younger moraines than ones within older moraines (see discussion below and Table 3).

The thick terraces on the outwash plains may also be related to the fluctuations in discharge of meltwater because of the large seasonal and diurnal temperature changes. Glaciofluvial or fluvial terraces are produced by allocyclic processes and climate changes throughout the Quaternary. They are often subsidiary, however, to terraces formed by other processes, such as morainic and lacustrine terraces.

The general assumption of very high sediment loads in mountain systems is valid for the region but sediment transfer is an episodic process associated with seasonal cycles and the dynamics of highly active hillslope processes. Around the region, the abundance of paraglacial landforms might be evidence for the episodic nature of sediment transfer. The importance of paraglaciation has been highlighted in other regions of the Himalayan–Tibetan orogen and elsewhere in the world (Ballantyne, 2002; Barnard et al., 2003, 2004a,b, 2006) and our study supports these views.

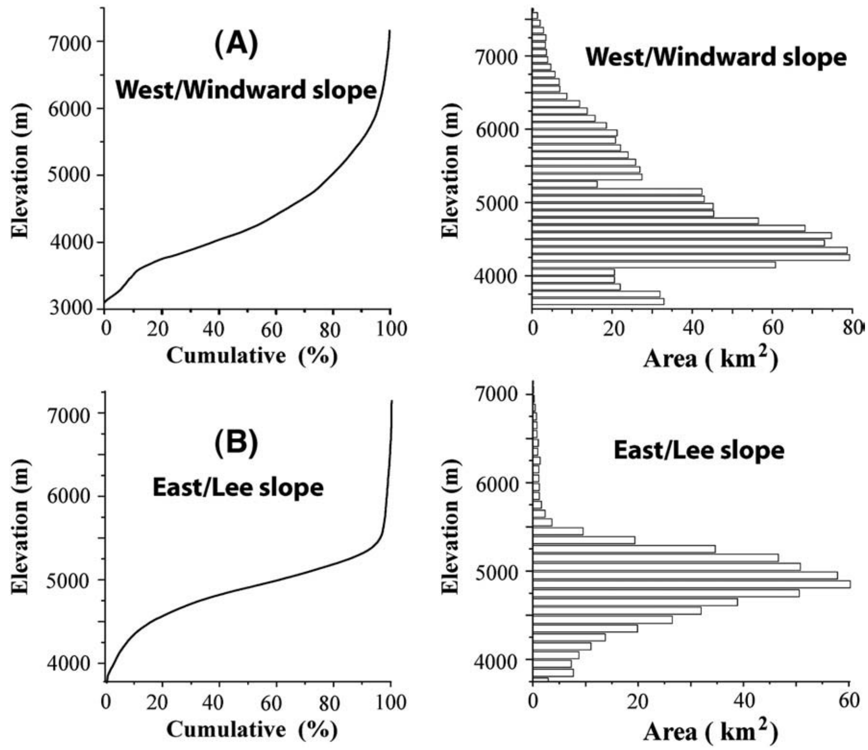

Fig. 24. The area-altitude distribution (hypsometry) and histograms across the high ridges of Muztag Ata. (A) is for west (windward) side and (B) for east (lee) side. The boundary of both sides is shown Fig. 23A.

7.4. Drainage basin and basin-wide rates of erosion

The plan-view drainage system is largely controlled by tectonics. Radial drainage in the headwaters from the two domes flows into the main Kengxuar River that parallels the Kongur detachment fault before cutting antecedent across the northern slopes of Kongur Shan and ultimately into the Tarim Basin. The two knick points that are identified, one at the moraine-dammed lake (Kara Kol) through hummocky moraine and the other just beyond the junction of Gez River and Kengxuwar River, are probably related to damming and tectonic uplift/subsidence, respectively (Whipple et al., 1999; Snyder et al., 2000). The first knickpoint (a in Fig. 15), at Kara Kol, likely relates to a base level change that resulted from moraine damming and the following incision. The knick point and gorge section at the Gez and Kengxuwar river confluence (b in Fig. 15) might be related to rapid incision that resulted from the increase in combined discharge and bedrock uplift along the Kongur detachment fault.

Although calculating rates of erosion for glaciated catchments is challenging, our data shows that the rate of erosion for samples collected proximal to young moraines, with 1st and 2nd order streams, is in the order of 540–1400 m/Ma. This is likely, however, to be an overestimate of the long-term rate of erosion, as substantial bedrock was removed during the Holocene glaciations of these valleys, essentially diluting the TCN concentrations. The higher order streams that were not, or were less glaciated during the Holocene provide lower estimates of the rates of erosion (22–100 m/Ma). It probably represent more effective basin-wide mixing of TCNs and are more likely representative of the average TCN concentration of adjacent, older moraines.

The low values (11–23 m/Ma) for bedrock weathering places a lower limit on denudation for the hanging wall. Despite the uncertainties inherent in using TCN concentrations for glaciated terrains, the data allow a broad estimate of the denudation of the region. For example, the difference in rate of erosion between 1st–2nd order streams and higher order streams demonstrates that sediment is not transferred rapidly downstream for the glaciated catchments. This suggests that the streams draining the catchment on the western slope of Muztag Ata are not very efficient in transferring sediment, at least on the timescale of 10^3–10^5 yr. Furthermore, the low rates of erosion determined for hanging wall bedrock in this study (11–23 m/Ma) and boulders on the oldest moraine (2–4 m/Ma) recalculated from Seong et al. (2007), show that weathering is not as important as glacial and fluvial erosion in this region. Furthermore, the lower values for the erosion of boulders, compared to bedrock, illustrate how resistant individual glacial boulders can be to weathering processes. This provides confidence when using boulders on moraines to define the ages of moraines and the timing of glaciation.

Many previous studies (Brown et al., 1995; Granger et al., 1996; Clapp et al., 2000, 2001; Bierman and Caffee, 2001; Schaller et al., 2001; Matmon et al., 2003) are based on a steady state erosion model for calculation of the basin-wide rates of erosion from TCN concentrations of riverine sediments. The other recent studies (Niemi et al., 2005; Stock et al., 2006) suggest that the contribution of TCN from different parts of the basin, however, is not equal, which is especially greatly influenced by landslides. A simulation study by Niemi et al. (2005) argued that basin-wide rates of erosion deduced from TCN concentration of sediments, has a decreasing tendency with an increasing ratio of landsliding to steady-state bedrock weathering. This might affect the study area, in which paraglacial and earthquake-related landslidings are frequent. Thus, we cannot rule out the possibility of underestimation of the true rate of erosion of the basin studied, resulting from the contribution of TCN of sediments newly exposed to cosmic rays by deep-seated landsliding.

Our rates of erosion contrast with the long-term rate of denudation determined from thermochronometric data (Arnaud et al., 1993), which is four to five times greater than the short-term rates of erosion determined from ^{10}Be TCN method. This is to be expected because to maintain high topography, uplift must exceed denudation. The variation in rates of erosion with the different time scales implies that Muztag Ata and Kongur Shan have not been in dynamic equilibrium

Table 3
The present equilibrium line altitudes (ELAs) and ELA depressions for Muztag Ata and Kongur Shan

Present ELAs (m)

	Contour	THAR [a] (0.5)	MELM[b]	Hypsometry	AAR[c] (0.44)	AAR (0.67)	BR[d] (2.0)	Aspect
Olimde-1	4440	5285	4400	4951	4962	4734	4756	N
Subax	5180	5448	4640	5222	5427	5245	5110	NW
Kmatolja	4840	5679	4800	5193	5985	5311	5433	NWW
Kartamak	4800	5313	4560	4923	5109	4787	4830	W
Rijek	5180	5211	5160	5416	5467	5225	5248	SWW
Uzuntal	4560	5530	4520	6065	6140	5715	5778	SWW
Tangi	4820	5613	4800	5935	6188	5780	5862	SWW
Kotakir	4840	5553	4760	6318	6263	5747	5907	SW
Kongurjiubie	4980	5939	4800	5196	5775	5126	5270	SW
Jangmanjar	4840	5707	4760	5354	5618	5391	5424	SW
Karayaylak	3920	4352	3880	3872	3888	3576	3660	NE
Kuksay	4320	5519	4640	4919	4898	4683	4712	NE
Qimgan	3920	4836	3900	4764	4743	3995	4116	E
BeiQimgan	3960	4182	3960	4012	4091	3852	3898	E
Tugraalkuluxi	3960	4468	3940	4338	4269	4063	4115	NE

ELA Lowering (m)

	Present[e]	LIA	1.5 ka	3.5 ka	4.2 ka	6.3 ka	8.0 ka	9.6 ka	10.6 ka	13 ka	16 ka	LG[f]	PG[g]
Olimde-1	4734	22	55			278				318	343		
Subax	5245											1223	
Kmatolja	5311				163								
Kartamak	4787	29						60		259			
Rijek	5525												1975
Uzuntal	5715			296		376			592			1573	
Tangi	5780	95											
Kotakir	5747											1596	
Kongurjiu	5126						1417						
Jangmanjar	5391						1354						
Karayaylak	3576	118											

THAR is tow to headwall ratio, MELM for maximum elevation of lateral moraine, AAR for accumulation area ratio, and BR is balance ratio.
[a] Toe to headwall ratio.
[b] Maximum elevation of lateral moraine.
[c] Accumulation area ratio.
[d] Balance ratio.
[e] The values from AAR of 0.67.
[f] The Last Glacial cycle.
[g] Penultimate Glacial cycle.

since the onset of rapid uplift at ~2 Ma. Furthermore, focused glacial erosion on the footwall and/or the sediment burden on the hanging wall because of retarded sediment redistribution, might enhance rock uplift of the footwall. The ^{10}Be TCN concentrations show that the rate of erosion from the basin constituting most of the hanging wall of the Kongur normal fault is five to ten times lower than the Himalayan area with similar glacier and tectonic setting (Vance et al., 2003). This discrepancy might result from inefficient sediment transfer by fluvial systems because of the low precipitation within the region. The lower value of the basin-wide rates of erosion, however, is in good agreement with dryland regions devoid of glaciers, such as the Negev Desert in Israel (Clapp et al., 2000).

In summary, clear spatial and temporal controls exist on landform distribution and formation in the Muztag Ata and Kongur Shan massifs. These are controlled primarily by tectonics, which in turn influences local climate, distribution of glaciers and their resultant controls on erosion and sediment transfer. Climatic oscillations result in fluctuating glaciers, which also influence other Earth surface processes. Major landscape changes likely result from readjustments during periods of deglaciation and during large seismic events. Landscape changes in this region are probably sporadic and occur very rapidly, mainly during deglaciation. The role of fluvial/glacio-fluvial sedimentation during paraglacial modification has still to be fully assessed, but clearly the erosion of moraines and resedimentation on outwash plains in association with moraines and alluvial fans are dramatic and important. Although the uplift history has yet to be fully quantified in detail by thermochronology and tectonic geomorphology, the strong spatial variability in topography and landform distribution suggests that a glacial buzz-saw model could explain the gross geomorphology of the massifs.

8. Conclusions

The geomorphic and tectonic evolution of the Muztag Ata and Kongur Shan region is the result of complex interactions between endogenetic and exogenic processes, resulting in rapid Quaternary uplift and concentrated incision. Tectonic uplift may have been enhanced by denudational unloading by glacial incision, but this has yet to be defined. Glaciation dominates the landform development, producing extensive successions of moraines and inducing paraglacial modification of the landscape by erosion and resedimentation. Glaciers have oscillated considerably throughout the Late Quaternary, with as many as eight advances during the Holocene alone. The style of glaciation has also changed in this region which resulted in glacial landforms typical of debris mantled glaciers to landforms typical of small, clean glaciers. Earthquake-induced catastrophic events, such as long-runout landslides, are important in landform formation in this region.

The topography and glacier forms in the Muztag Ata and Kongur Shan massifs vary across a broadly N–S trending high ridge and watershed. The western portion, situated on the windward slope has gentle high topography and small valley glaciers, while on the eastern, leeward slopes, gradients are steeper and long debris-covered valley glaciers are present. The hypsometry of the region showed two peaks in the distribution frequency of elevation at 3600–4100 m and 4400–4800 m asl (Fig. 24). The two frequent elevation zones are consistent with the former equilibrium line altitudes during the Olimde and Subaxh glacial stages. This helps support the buzz-saw hypothesis that glaciers determine hypsometry by means of rapid erosion at the ELA.

Basin-wide rates of erosion range from ~0.1 to 1.4 km/Ma based on our TCN analysis, and is an order of magnitude lower than the rate of exhumation of both massifs in the footwall of the Kongur detachment (4–6 km/Ma). The discrepancy between two methods with different time scales suggests that the landscape is not in dynamic equilibrium and/or might indicate that uplift was initially very rapid and has slowed during the Late Quaternary. The glacial erosion focused on the footwall of the detachment fault likely enhanced topography through isostatic peak uplift and compensatory flow.

Acknowledgements

We would like to thank Professors Jack Vitek, Glenn Thackray, Milap Sharma and Zhang Wei for their useful and constructive reviews of our paper. Particular thanks go to Chinese colleagues (Yabing Li, Gongbi Chen, Ming Chen, and Jianyi Dong) for their help in the field and greatly acknowledge support for fieldwork from the National Science Foundation of China (NSFC Grant 40571021). This work was undertaken at the Lawrence Livermore National Laboratory (LLNL) (under DOE contract W-7405-ENG-48) as part of an Institute of Geophysics and Planetary Physics/Lawrence Livermore National Laboratory (IGPP/LLNL) research grant.

References

Aizen, V., Aizen, E., 1997. Hydrological cycles on the north and south peripheries of mountain-glacial basins of Central Asia. Hydrological Processes 11, 451–469.

Aizen, E.M., Aizen, V.B., Melack, J.M., Nakamura, T., Ohta, T., 2001. Precipitation and atmospheric circulation patterns at mid-latitudes of Asia. International Journal of Climatology 21, 535–556.

Andrews, J.T., 1972. Glacier power, mass balances, velocities, and erosion potential. Zeitschrift fűr Geomorphologie 13, 1–17.

Andrews, J.T., 1975. Glacial Systems: An approach to glaciers and their environments. Wadsworth Pub., Duxbury, London.

Arnaud, N.O., Brunel, M., Cantagrel, J.M., Tapponnier, P., 1993. High cooling and denudation rates at Kongur Shan, eastern Pamir (Xinjiang, China) reavealed by $^{40}Ar/^{39}Ar$ alkali feldspar thermochronology. Tectonics 12, 1335–1346.

Ballantyne, C.K., 2002. A general model of paraglacial landscape response. The Holocene 12 (3), 371–376.

Barnard, P.L., Owen, L.A., Sharma, M.C., Finkel, R.C., 2001. Natural and human-induced landsliding in the Garhwal Himalaya of Northern India. Geomorphology 40, 21–35.

Barnard, P.L., Owen, L.A., Finkel, R.C., Asahi, K., 2003. Landscape response to deglaciation in a high relief, monsoon-influenced alpine environment, Langtang Himal, Nepal. Quaternary Science Riviews 25, 2162–2176.

Barnard, P.L., Owen, L.A., Finkel, R.C., 2004a. Style and timing of glacial and paraglacial sedimentation in a monsoonal influenced high Himalayan environment, the upper Bhagirathi Valley, Garhwal Himalaya. Sedimentary Geology 165, 199–221.

Barnard, P.L., Owen, L.A., Sharma, M.C., Finkel, R.C., 2004b. Late Quaternary landscape evolution of a monsoon-influenced high Himalayan valley, Gori Ganga, Nanda Devi, NE Garhwal. Geomorphology 61, 91–110.

Barnard, P.L., Owen, L.A., Finkel, R.C., 2006. Quaternary fans and terraces in the Khumbu Himal south of Mount Everest: their characteristics, age and formation. Journal of Geological Society of London 163 (2), 383–399.

Barrows, T.T., Stone, J.O., Fifield, L.K., Cresswell, R.G., 2002. The timing of the Last Glacial Maximum in Australia. Quaternary Science Reviews 21, 159–173.

Barry, R.G., Chorley, R.J., 2003. Atmosphere, weather, and climate, 8th ed, p. 279.

Benn, D.I., Lehmkuhl, F., 2000. Mass balance and equilibrium-line altitudes of glaciers in high mountain environments. Quaternary International 65/66, 15–29.

Benn, D.I., Owen, L.A., Osmaston, H.A., Seltzer, G.O., Porter, C.S., Mark, B., 2005. Reconstruction of equilibrium-line altitudes for tropical and sub-tropical glaciers. Quaternary International 138/139, 230–243.

Bierman, P.R., Steig, E.J., 1996. Estimating rates of denudation using cosmogenic isotope abundances in sediment. Earth Surface Processes and Landforms 21, 125–139.

Bierman, P.R., Caffee, M., 2001. Steady state rates of rocks surface erosion and sediment production across the hyperarid Namib Desert and the Namibian escarpment, southern Africa. American Journal of Science 301, 326–358.

Bishop, M.P., Shroder, J.F., Ward, J.L., 1995. SPOT multispectral analysis for producing supraglacial debris-load estimates for Batura Glacier, Pakistan. Geocarto Internationl 10 (4), 81–90.

Bishop, M.P., Bonk, R., Kamp, U., Shroder, J.F., 2001. Topographic analysis and modeling for alpine glacier mapping. Polar Geography 25, 182–201.

Brocklehurst, S.H., Whipple, K.X., 2002. Glacial erosion and relief production in the Eastern Sierra Nevada, California. Geomorphology 42, 1–24.

Brocklehurst, S.H., Whipple, K.X., 2004. Hypsometry of glaciated landscapes. Earth Surface Processes and Landforms 29, 907–926.

Brown, E., Stallard, R.F., Larsen, M.C., Raisbeck, G.M., Yiou, F., 1995. Denudation rates determined from the accumulation of in situ-produced ^{10}Be in the Luquillo Experimental Forest, Puerto Rico. Earth and Planetary Science Letters 129, 193–202.

Brozovich, N., Burbank, D.W., Meigs, A.J., 1997. Climatic limits on landscape development in the northwestern Himalaya. Science 276, 571–574.

Brunel, M., Arnaud, N., Tapponnier, P., Pan, Y., Wang, Y., 1994. Kongur Shan normal fault: Type example of mountain building assisted by extension (Karakoram fault, eastern Pamir). Geology 22, 707–710.

Clapp, E.M., Bierman, P.R., Schick, A.P., Lekach, J., Enzel, Y., Caffee, M., 2000. Sediment yield exceeds sediment production in arid region drainage basins. Geology 28, 995–998.

Clapp, E.M., Bierman, P.R., Nichols, K.K., Pavich, M., Caffee, M., 2001. Rates of sediment supply to arroyos from upland erosion determined using in situ produced cosmogenic ^{10}Be and ^{26}Al. Quaternary Research 55, 235–245.

Derbyshire, E., 1981. Glacier regime and glacial sediment facies: a hypothetical framework for the Qinghai–Xizang Plateau. Proceedings of Symposium on Qinghai–Xizang (Tibet) Plateau, Beijing, China. Geological and Ecological studies of Qinghai–Xizang Plateau, vol. 2. Science Press, Beijing, pp. 1649–1656.

Denton, G.H., Heusser, C.J., Lowell, T.V., Moreno, P.I., Anderson, B.G., Heusser, L.E., Schlüchter, C., Marchant, D.R., 1999. Interhemispheric linkage of paleoclimate during the last glaciation. Geografiska Annaler 81A, 107–154.

Duncan, C.C., Klein, A.J., Masek, J.G., Isacks, B.L., 1998. Late Pleistocene and modern glaciations in Central Nepal from digital elevation data and satellite imagery. Quaternary Research 49, 241–254.

Fort, M., Peulvast, J., 1995. Catastrophic Mass-movements and Morphogenesis in the Peri–Tibetan Ranges: Examples for West Kunlun, East Pamir and Ladakh. In: Slaymaker, O. (Ed.), Steepland Geomorphology, pp. 171–198.

Granger, D.E., Kirchner, J.W., Finkel, R., 1996. Spatially averaged long-term erosion rates measured from in-situ produced cosmogenic nuclide in alluvial sediments. Journal of Geology 104, 249–257.

Kääb, A., Huggel, C., Paul, F., Wessels, R., Raup, B., Kieffer, H., Kargel, J., 2002. Glacier monitoring from ASTER imagery: accuracy and applications. EARSeL Proceedings. LISSIGWorkshop, Berne.

Kaufman, D.S., Porter, S.C., Gillespie, A.R., 2004. Quaternary alpine glaciations in Alaska, the Pacific Northwest, Sierra Nevada, and Hawaii. In: Gillespie, A.R., Porter, S.C., Atwater, B.F. (Eds.), The Quaternary Period in the United States. Developments in Quaternary Science, vol. 1, pp. 77–104.

Kohl, C.P., Nishiizumi, K., 1992. Chemical isolation of quartz for measurement of in-situ produced cosmogenic nuclides. Geochimica et Cosmochimica Acta 56, 3583–3587.

Koons, P., 1994. Three-dimensional critical wedges: tectonics and topography in oblique collisional orogens. Journal of Geophysical Research 99 (B6), 12301–12315.

Lal, D., 1991. Cosmic ray labeling of erosion surfaces: in situ nuclide production rates and erosion models. Earth and Planetary Science Letters 104, 429–439.

Lanzhou Institute of Glaciology and Geocryology, 1994. The topographic map of Kongur Tagh-Muztag Ata.

Liu, Q., 1993. Paleoclimat et contrainte chronologiques sur les mouvements recents dans l-ouest du Tibet: failles due Karakorum et de Longmu Co-Gozha Co, lacs en Pull-Apart de Longmu Co et Sumxi Co. These de Doctorat, Universite Paris 7. pp. 360.

Matmon, A., Bierman, P.R., Larsen, J., Southworth, S., Pavich, M., Caffee, M., 2003. Temporally and spatially uniform rates of erosion in the southern Appalachian Great Smoky Mountains. Geololgy 31 (2), 155–158.

Meigs, A., Sauber, J., 2000. Southern Alaska as an example of the long-term consequences of mountain building under the influence of glaciers. Quaternary Science Reviews 19, 1543–1562.

Miehe, G., Winiger, M., Bohner, J., Yili, Z., 2001. Climatic diagram map of high Asia. Purpose and concepts. Erdkunde 55, 94–97.

Mitchell, S.G., Montgomery, D.R., 2006. Influence of a glacial buzzsaw on the height and morphology of the Cascade Range in central Washington State, USA. Quaternary Research 65, 96–107.

Molnar, P., England, P., 1990. Late Cenozoic uplift of mountain ranges and global climate change: Chicken or egg? Nature 346, 29–34.

Montgomery, D.R., Balco, G., Willett, S.D., 2001. Climate, tectonics and the morphology of the Andes. Geology 29, 579–582.

Niemi, N.A., Oskin, M., Burbank, D.W., Heimsath, A.M., Gabet, E.J., 2005. Effects of bedrock landslides on cosmogenically determined erosion rates. Earth and Planetary Science Letters 237, 480–498.

Nishiizumi, K., Imamura, M., Caffee, M.W., Southon, J.R., Finkel, R.C., McAninch, J., 2007. Absolute calibration of 10Be AMS standards. Nuclear Instruments and Methods in Physics Research Section B258 (2), 403–413.

Ohmura, A., Kasser, P., Funk, M., 1992. Climate at the equilibrium line of glaciers. Journal of Glaciology 15, 403–415.

Ono, Y., Liu, D., Zhao, Y., 1997. Paleoenvironments of Tibetan Plateau from glacial fluctuations in the northern foot of the West Kunlun Mountains. Journal of Geography 106, 184–198 (Japanese).

Owen, L.A., Derbyshire, E., 1989. The Karakoram glacial depositional system. Zeitschrift für Geomorphologie 76, 33–73.

Owen, L.A., England, J., 1998. Observations on rock glaciers in the Himalayas and Karakoram Mountains of northern Pakistan and India. Geomorphology 26, 199–213.

Owen, L.A., Benn, D.I., 2005. Equilibrium-line altitudes of the Last Glacial Maximum for the Himalaya and Tibet: an assessment and evaluation of results. Quaternary International 138/139, 55–78.

Owen, L.A., Finkel, R.C., Barnard, P.L., Haizhhou, M., Asahi, K., Caffee, M.W., Derbyshire, E., 2005. Climatic and topographic controls on the style and timing of Late

Quaternary glaciation throughout Tibet and the Himalaya defined by ^{10}Be cosmogenic radionuclide surface exposure dating. Quaternary Science Reviews 24, 1391–1411.
Owen, L.A., Caffee, M.W., Bovard, K.R., Finkel, R.C., Sharma, M.C., 2006. Terrestrial cosmogenic nuclide surface exposure dating of the oldest glacial successions in the Himalayan orogen. Ladakh Range, northern India. Geological Society of America Bulletin 118, 383–392.
Porter, S.C., 1989. Some geological implications of average Quaternary glacial conditions. Quaternary Research 32, 245–261.
Robinson, A.C., 2005. Tectonic evolution of the Kongur Shan extensional system, northeastern Pamir: Implications for the evolution of the western Himalayan–Tibetan orogen. Ph.D thesis, University of California, Los Angels. pp. 333.
Robinsion, A.C., Yin, A., Manning, C.E., Harrison, T.M., Zhang, S.H., Wang, X.F., 2004. Tectonic evolution of the north eastern Pamir: Constraints from the portion of the Cenozoic Kongur Shan extensional system, western China. Geological Society of America Bulletin 116 (7/8), 953–973.
Schaller, F., von Blanckenburg, N., Kubik, P.W., 2001. Large-scale erosion rates from in situ-produced cosmogenic nuclides in European river sediments. Earth and Planetary Science Letters 188, 441–458.
Schoenbohm, L., Chen, J., Sobel, E., Thiede, R., Strecker, M., 2005. Glacial erosion, deep exhumation and the *development* of high topography along the Kongur detachment, Pamir Mountains, Western China. Eos Trans (Transactions, American Geophysical Union) 86 (52), T23C–0576.
Seong, Y.B., Owen, L.A., Yi, C., Finkel, R., 2007. Late Quaternary glaciation of Muztag Ata and Kongur Shan in the semi-arid region of northwestern Tibet. Geological Society of America Bulletin In submission.
Shi, Y., 2002. Characteristics of late Quaternary monsoonal glaciation on the Tibetan Plateau and in East Asia. Quaternary International 97/98, 79–91.
Shroder, J.F., Scheppy, R.A., Bishop, M.P., 1999. Denuation of small alpine basins, Nanga Parbat Himalaya, Pakistan. Arctic, Antarctic, and Alpine Research 31, 121–127.
Shroder, J.F., Bishop, M., Copland, P.L., Sloan, V.F., 2000. Debris-covered glaciers and rock glaciers in the Nanga Parbat Himalaya, Pakistan. Geografisca Annaler 82A, 17–31.
Singer, B.S., Ackert, R.P., Guillou, H., 2004. $^{40}Ar/^{39}Ar$ and K–Ar chronology of Pleistocene glaciations in Patagonia. Geological Society of America Bulletin 116, 434–450.
Skrine, C.P., 1925. The alps of Qungur. The Geographical Journal 66 (5), 385–407.
Smith, J.A., Farber, D.L., Seltzer, G.O., Finkel, R.C., Rodbell, D.T., 2002. Chronology of tropical glaciation from cosmogenic dating. Eos (Transactions, American Geophysical Union) 83 (47), F922.
Snyder, N.P., Whipple, K.X., Tucker, G.E., Merritts, D.J., 2000. Landscape response to tectonic forcing: DEM analysis of stream profiles in the Mendocino triple junction region, northern California. Geological Society of America Bulletin 112, 1250–1263.
Spotila, J.A., Buscher, J.T., Meigs, A.J., Reiners, P.W., 2004. Long-term glacial erosion of active mountain belts: Example of the Chugach–St. Elias Range, Alaska. Geology 32 (6), 501–504.
Stock, G.M., Ehlers, T.A., Farley, K.A., 2006. Where does sediment come from? Quantifying catchment erosion with detrital apatite (U–Th)/He thermochronometry. Geology 34, 725–728.
Stone, J.O., 1999. A consistent Be-10 production rate in quartz — muons and altitude scaling. AMS-8 Proceedings Abstract Volume, Vienna, Austria.
Stone, J.O., 2000. Air pressure and cosmogenic isotope production. Journal of Geophysical Research 105 (B10), 23753–23759.
Strahler, A.N., 1952. Dynamic basis of geomorphology. Geological Society of America Bulletin 63, 923–938.
Vance, D., Bickle, M., Ivy-Ochs, S., Kubik, P.W., 2003. Erosion and exhumation in the Himalaya from cosmogenic isotope inventories of river sediments. Earth and Planetary Science Letters 206, 273–288.
Wake, C.P., Mayewski, P.A., Han, J., 1994. Modern eolian dust deposition in Central Asia. Tellus 46B, 220–233.
Whipple, K., Kirby, E., Brocklehurst, S., 1999. Geomorphic limits to climate-induced increases in topographic relief. Nature 401, 39–43.
Zech, R., Abramowki, U., Glaser, B., Sosin, P., Kubik, P.W., Zech, W., 2005. Late Quaternary glacial and climate history of the Pamir Mountains derived from cosmogenic ^{10}Be exposure ages. Quaternary Research 64, 212–220.